Calcium Excess in Novae: Beyond Nuclear Physics Uncertainties

by

Mallory Loria
B.Sc., University of Waterloo, 2022

A Thesis Submitted in Partial Fulfillment of the
Requirements for the Degree of

MASTER OF SCIENCE

in the Department of Physics and Astronomy

Calcium Excess in Novae: Beyond Nuclear Physics Uncertainties

by

Mallory Loria
B.Sc., University of Waterloo, 2022

Supervisory Committee

Dr. F. Herwig , Co-supervisor
(Department of Physics and Astronomy)

Dr. C. Ruiz , Co-supervisor
(Department of Physics and Astronomy/ TRIUMF)

Abstract

We examine Ca abundances in classical novae from spectroscopic observations spanning 65 years and investigate whether they are systematically high compared to those predicted by nova models. For the first time, we perform Monte Carlo simulations assessing the impact of nuclear reaction rate uncertainties on abundances predicted by multi-zone nova models. We compare these results with similar simulations using one-zone nova models. While the Ca abundances in the models are sensitive to variations of rates of the reactions $^{37}\mathrm{Ar}(p,\gamma)^{38}\mathrm{K}$ and $^{38}\mathrm{K}(p,\gamma)^{39}\mathrm{Ca}$, the nuclear physics uncertainties of these reactions cannot account for the discrepancy between the observed and predicted Ca abundances in novae. We also investigate the impact of the $^{19}\mathrm{F}(p,\gamma)/^{19}\mathrm{F}(p,\alpha)$ branching ratio that controls hot CNO cycle breakout on Ca production by increasing this ratio by factors of 10 and 100, finding no increase in the Ca abundance. To explain the peculiar abundances observed in novae with high Ca abundances, alternative mixing scenarios with different pre-mixed material are explored. The dust fractionation hypothesis, which suggests that the Ca overabundance could be explained by Ca being trapped in dust, is ruled out due to the simultaneous overabundance of Ar, which would not be expected to be trapped in dust. Furthermore, the overabundance of Ca has important implications for measuring ^{7}Be in nova ejecta, as Ca lines are used to estimate ^{7}Be abundances. If the Ca abundance is incorrectly determined, it could lead to inaccurate ^{7}Be abundance estimates. Possible alternative explanations for the observed Ca overabundance are discussed.

Table of Contents

List of Tables

List of Figures

Acknowledgements

They say it takes a village and I am so lucky to have found mine. I am truly thankful to all of you who have shown me love, kindness, support, and patience. I would not be here without you. Thank you from the bottom of my heart.

I am deeply grateful for my supervisors Dr. Falk Herwig and Dr. Chris Ruiz. They have truly made this degree such a fantastic experience and provided a place that allowed for my passion to grow and my skills to develop. Thank you for your guidance, support, and kindness. Thank you for always being willing to make time for me, believing in me, encouraging me, normalizing the struggle of grad school, and sharing your knowledge with me. I am very lucky to have learned from you and to keep learning from you.

To Dr. Pavel Denissenkov, 1000 thank you's wouldn't be enough. Your patience, kindness, and support made this work possible. Thank you for answering all my questions, even the silly ones, and thank you for our discussions, I thoroughly enjoy them and am so grateful to work with you.

I especially want to thank my family, mainly my mom, my sister, and my Opa. Mom, thank you for always picking me back up when I need it. Thank you for constantly reminding me that I am strong, can do this, and that I do not have to do this alone. Thank you for making me who I am and giving me the tools I need to succeed. Ava, thank you for making me laugh and cheering me up whenever I need it, and thank you for keeping me grounded. Opa, thank you for teaching me math and passing on your genius.

To my best friend Wilfred, thank you for creating a place for me to be truly and unabashedly myself, in doing so you have helped me flourish. Thank you for hugging me on bad days and celebrating with me on good ones. I would also like to thank you for being my in-house data scientist. Our discussions on coding and statistics have helped enormously. Most importantly, thank you for always listening.

To my grade nine English teacher. Thank you for letting me do my book report on stars, who knew things would get this far? Thank you for believing in me and never letting me doubt myself. You cultivated my curiosity and made me hate English less.

To Sim, Olha, Carlos, Olivia, Chris, Aviv, Sam, Monika, and Izzy thank you for getting me through my undergrad and into grad school, for being patient with me, and for picking up the phone whenever I need you. I don't know what I would do without you. To Annabelle, Dan, Alex, Serene, and Jackie. Thank you for making Vancouver awesome and getting me out of the house. To Dr. Annika Lennarz at TRIUMF, thank you for having my back, being my sounding board and role model, and keeping me sane. I appreciate you immensely.

I acknowledge and respect the traditional, ancestral, and unceded territory of the Musqueam people, who for millennia have passed on their culture, history, and traditions from one generation to the next on this site on whose territories I work and live. I also acknowledge, with respect, the Lekwungen-speaking peoples on whose traditional territory the university stands and the Songhees, Esquimalt and WSÁNEĆ peoples whose historical relationships with the land continue to this day

Dedication

To my Mom:
For showing me what it means to be resilient.

Chapter 1

Introduction

1.1 Motivation

Classical novae are explosive H-burning events that occur in binary systems with a primary white dwarf (WD) and a secondary main sequence (MS) or evolved companion star. Classical novae are among the most common types of stellar explosions in our galaxy, with approximately 20–70 occurring each year (Shafter, 2017a). These eruptions on the surface of the WD are highly luminous and are often observed in UV, optical, and X-ray wavelengths, with the spectra from these events providing detailed information about the chemical abundances. Fig. 1.2 shows the ejected envelope following the explosion as seen in X-ray wavelengths. The temperature of these explosions is dependent on the initial conditions of the system and typically reaches a peak temperature of 2–4$\times10^8$K (Denissenkov et al., 2013) with some extreme novae having temperatures reaching sufficiently high levels to enable the production of heavy elements. As a result of these explosions, heavy element-enriched material is ejected into the environment surrounding the nova system, whether that is the interstellar medium or the interior of globular clusters. Novae are significant contributors to the galactic chemical abundance and evolution of certain elements, such as Li (Izzo et al., 2015). The energies at which these nuclear reactions occur can be replicated in laboratories, making novae excellent motivators for studying charged-particle reactions experimentally. Novae have recently been classified as gamma-ray emitting sources (Ackermann et al., 2014), which was unexpected, as for this to happen, particles must be accelerated to incredibly high energies. This new insight has reinvigorated the field by prompting a reevaluation of our models and understanding of these systems. Despite their prevalence, many aspects of novae remain poorly understood, including the mixing mechanisms between the WD and accretion disk, the hydrodynamics of the explosion, and the disruption of the disk. Novae are important to study because they are relatively simple compared to other explosive events such as core-collapse supernovae. For

instance, the explosion mechanism in novae, which involves the ignition of a thermonuclear runaway (TNR) in the outer layers, is simpler than that of core-collapse supernovae, which involve core collapse and neutrino shocks throughout the entire star. This simplicity allows them to serve as valuable models for understanding explosive nucleosynthesis and stellar physics.

In some nova observations, Ca is overabundant compared to solar values, which is unexpected since Ca is the assumed stopping point for nucleosynthesis in extreme novae (José & Hernanz, 2007a). When compared with the models of novae in this work, Ca was also found to be overabundant. The purpose of this work is to investigate whether the nuclear physics uncertainties in these models can account for this discrepancy.

1.2 Classical Novae

Classical novae, or novae for short, come from the Latin word *stella nova* meaning new star. Novae have been observed throughout history, but only in the early 20$^{\text{th}}$ century was a distinction made between classical novae and supernovae (Shapley, 1917). Theories of novae were highly speculative up until the mid-20$^{\text{th}}$ century when explanations involving binarity and the TNR were first presented (Bode & Evans, 2008).

It has been estimated that, for solar-type stars, the relative frequency of stars in a binary system is approximately 38% (Duquennoy & Mayor, 1991). Cataclysmic variables are a class of close binary systems with short orbital periods (Warner, 1995) involving mass transfer between a low-mass MS companion and a primary WD and are characterized by periodic eruptions and changes in luminosity. Classical novae are a subset of cataclysmic variables in which an explosion occurs due to H-burning on the surface of the WD, meaning that cataclysmic variables are the progenitors of classical novae. The primary star in a cataclysmic variable will evolve first, before the secondary companion, and will follow the typical stages of stellar evolution, as shown in Fig. 1.1. It will spend most of its life on the MS, burning H in its core until the H is exhausted; then it will evolve off the MS, and depending on its initial mass, it may become a red giant or a supergiant. If the star is within the appropriate mass range, it will experience an asymptotic giant branch (AGB) phase, characterized by thermal pulses and mass loss (Herwig, 2005). Eventually, the outer layers are expelled forming a planetary nebula, and the remaining core becomes a hot, compact, WD. The secondary star in the binary is typically a low-mass MS star; however, it can also be more evolved, like a red giant. As the secondary companion evolves more, it will eventually fill its Roche lobe. Either due to expansion and mass loss or due to a change in the Roche lobe limits of the binary

system, mass will be transferred from the companion to the WD. The mass transfer rate between the companion and the WD depends on several factors such as the orbital period, the type of mass transfer, properties of the WD, and magnetic fields Bode & Evans (2008).

There are several different types of novae other than classical. For example, recurrent novae are novae that erupt multiple times on the human time scale. Since the explosion does not destroy the binary system, after a period of quiescence, accretion will resume again. Technically all novae are recurrent; only some are not on the human time scale. Embedded novae are novae that tend to have longer orbital periods (Mikolajewska, 2010) and a secondary companion that is evolved, such as a red giant or other. The binary system of embedded novae usually transfers mass by stellar winds, as opposed to Roche lobe overflow, due to the large orbital period and, therefore, separation between the two. Symbiotic novae are a subset of embedded novae in which the evolution of the explosion takes place over very long time scales compared to their classical counterparts (Kenyon & Truran, 1983). Henceforth, any reference to novae refers to classical novae, which are the focus of this work.

Depending on the initial mass of the primary star, the WD in these systems is composed of either Carbon-Oxygen (CO) or Oxygen-Neon (ONe). The initial mass determines its evolutionary path and the type of nuclear burning that will take place. While all stars begin by burning H and then He, only more massive stars proceed to C-burning and beyond. Zero-age main sequence (ZAMS) stars with $M_{\rm ZAMS} \gtrapprox 7$–$8\,{\rm M}_\odot$ are expected to result in CO WDs, whereas ZAMS stars with masses in the range 7–$8\,{\rm M}_\odot \lessapprox M_{\rm ZAMS} \lessapprox 9$–$10\,{\rm M}_\odot$ are expected to produce ONe WDs (Doherty et al., 2015). These mass ranges are only estimates, as other factors contribute to the rate of nuclear burning, such as mass loss and mixing. For example, Chen et al. (2014) found that the C-burning rate (CBR) and the level of convective boundary mixing influence the initial mass required for CO WD formation. Specifically, the authors found the maximum initial mass for the formation of CO WDs increased from $M_{\rm i} \approx 5.5$ ${\rm M}_\odot$to $M_{\rm i} \gtrsim 7.0$ ${\rm M}_\odot$, depending on the CBR factor. The type of WD has important implications for the peak temperature that can be achieved in the TNR, as will be discussed later in the introduction.

The TNR in classical novae is initiated through the accretion of H-rich material onto the WD from its binary companion via Roche-lobe overflow. The Roche lobe in a binary system defines the region within which matter will be gravitationally bound to that star. At the inner Lagrangian point, there is no net force, as the gravitational and centrifugal forces cancel out. A depiction of the Roche lobe limits in a binary system can be seen in Fig. 1.2. Due to its angular momentum, the accreted material cannot be deposited directly onto the surface of the WD, so an accretion disk is formed around the WD. As more material

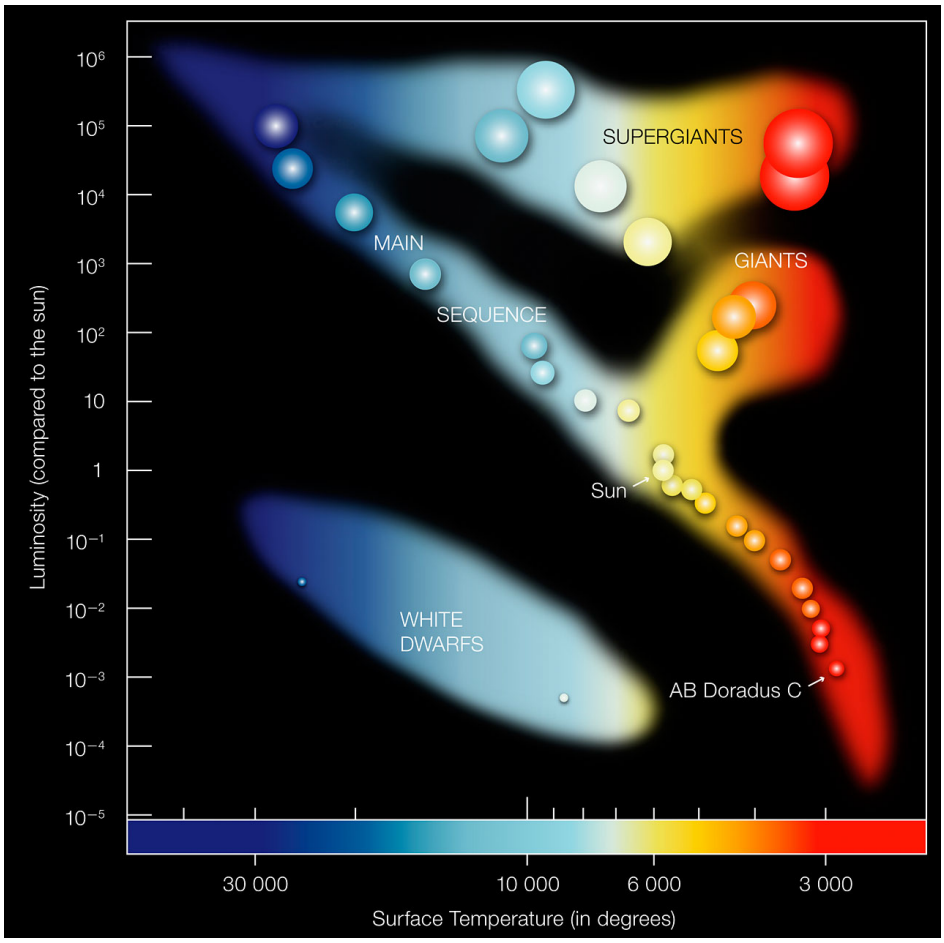

Figure 1.1: Hertzprung-Russell Diagram which shows the temperatures and luminosities of stars as they evolve. Image taken from European Southern Observatory (2007)

is accreted, a H-rich layer forms on the surface of the WD and gets compressed, causing the pressure, temperature, and density at the bottom of this layer to increase. When the temperature increases, the rate of nuclear burning also increases, until a peak temperature is reached and the electron degeneracy is lifted, enabling the outward explosion. The recurrence timescale for all novae is defined as the time it takes to accrete enough mass to achieve a TNR, $\tau_{\rm rec} = M_{\rm env}/M_{\rm acc}$ where $M_{\rm env}$ is the mass of the accreted envelope required to ignite the TNR and $M_{\rm acc}$ is the accretion rate. This time is usually between 10^4 and 10^7 years but in some extreme cases of recurrent novae, it can be as short as one year (Chomiuk et al., 2021). The actual TNR lasts for seconds to minutes, whereas the expansion and mass loss can last for days to months after which there will be a period of quiescence before the process repeats. Therefore, for classical novae the cycle repeats roughly every 10^4 and 10^7 years.

Specific details of stellar burning and the nova explosion will be discussed below.

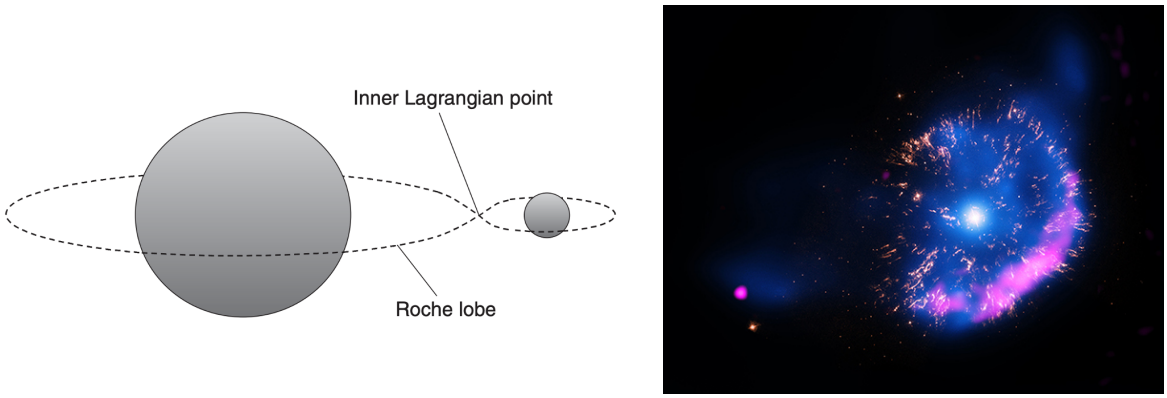

Figure 1.2: Depiction of Roche lobe limit in a binary system (left) from Iliadis (2015). Chandra X-ray image of nova GK Per 2015 from NASA/CXC/RIKEN/D.Takei et al. (2015).

1.2.1 Stellar Burning and Thermonuclear Runaway Explosions

Nuclear burning in novae occurs in distinct phases, each characterized by different dominant reaction sequences. During the initial accretion phase, when temperatures are relatively low, H-burning proceeds primarily through the proton-proton (pp) chain. As the temperature and density at the base of the accreted layer increase, the dominant energy production mechanism shifts from the pp chain to the Carbon-Nitrogen-Oxygen (CNO) cycle (Iliadis, 2015). This transition occurs because the CNO cycle is more efficient than the pp chain at these higher temperatures.

Several factors substantially influence the peak temperature of these explosions and thus the extent of nucleosynthesis that occurs. These factors include the WD type, mass, accretion rate, and central temperature. A hotter peak temperature increases the probability of producing heavy elements like Ca. The impact of these parameters will be discussed in detail below.

Observations of novae show enhancement in heavy elements, suggesting that nuclear burning alone cannot produce these abundance patterns (Gehrz et al., 1998). It is widely accepted in the nova community that there must be some level of mixing between the surface of the WD and the accreted layer to match the observations. The exact details of this mixing are still an active area of research. The WD type is important because it dictates the type of heavy element material that is mixed and burned. If the material at the base of the accreted envelope is more enriched in heavier elements like O and Ne (as opposed to C and O), heavier elements will be more likely to form during the TNR.

Through surface gravity, the WD mass plays an important role in determining the peak temperature reached during the TNR. The low surface gravity of a low-mass WD results in

lower pressure at the base of the accreted layer, making the material less electron degenerate and more similar to an ideal gas. As a result, for very low mass WDs, the peak TNR temperature may not reach high enough temperatures for heavy element nucleosynthesis to occur. Very degenerate material, however, does not expand as easily, meaning that higher TNR temperatures may be reached.

Highly degenerate material is key for a strong TNR. Without sufficient degeneracy, the temperatures cannot build up to the high values. If a large amount of mass is accreted very quickly, above $\sim 10^{-8}$ $M_\odot$ yr^{-1} (Bode & Evans, 2008), the temperature will rise faster due to compressional heating and the material will not be degenerate enough for a strong explosion. For this reason, more extreme novae are expected to have slower accretion rates. Fig. 1.3 further illustrates this point.

The central temperature of these WDs also impacts the amount of mass accreted before the explosion. If the central temperature of the WD is very hot, it will cause the accreted material to heat faster, which can lead to H-burning at the same rate as accretion, and no TNR will occur. Instances of this can be seen in H-shell flashes on the surface of massive, rapidly accreting WDs (Paczynski & Zytkow, 1978; Sion et al., 1979; Fujimoto & Taam, 1982).

Fig. 1.3 provides a visual summary of the parameters discussed in this section and their impact on the nova explosion. To summarize, the ingredients for an extreme nova explosion are a high-mass, cool ONe WD with a low accretion rate.

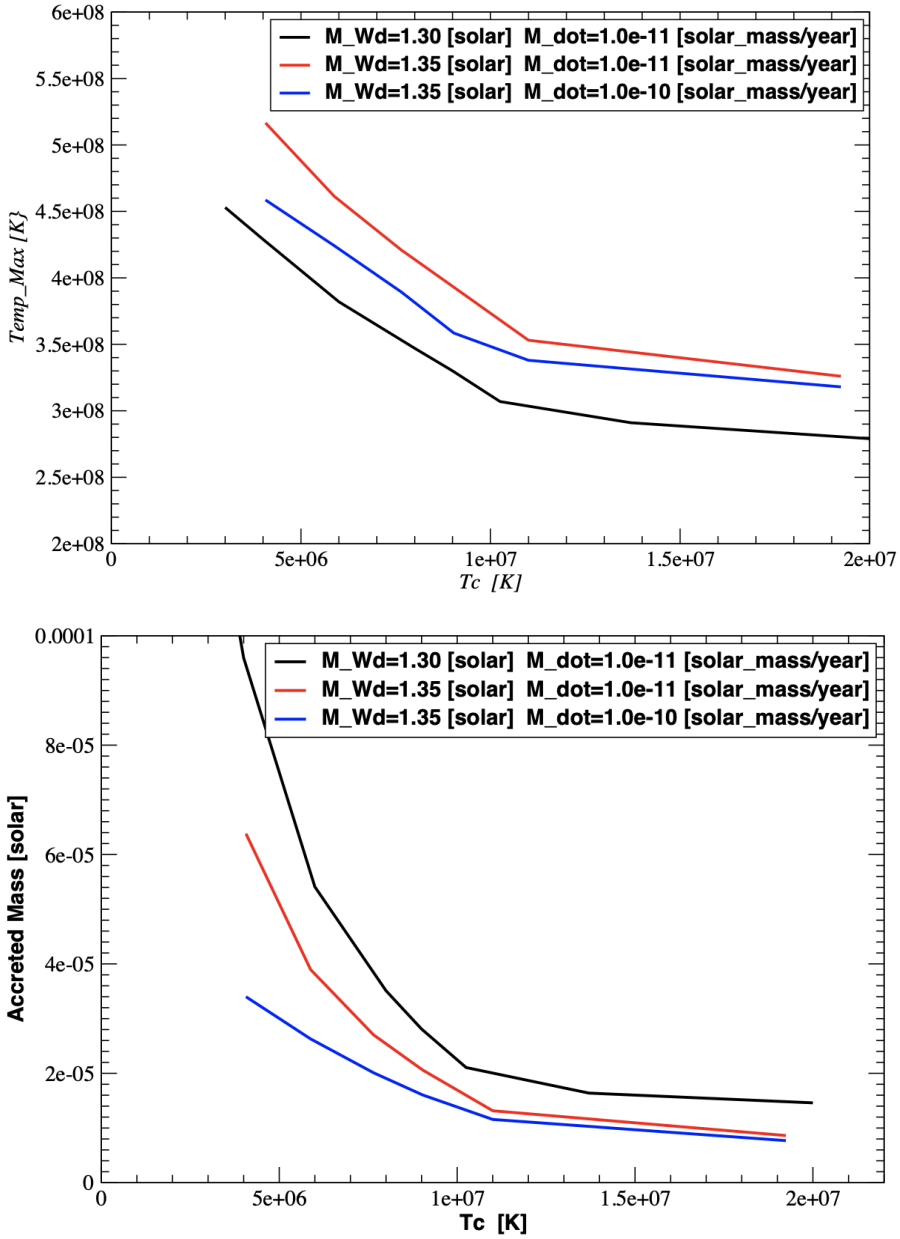

Figure 1.3: Nova characteristics based on WD central temperature, mass, and accretion rate (Glasner & Truran, 2009). Top panel: Maximum temperature reached during TNR. Bottom panel: Total mass accreted before explosion.

1.2.2 Observations of Novae

The primary observables of the WD in the nova system include the composition of ejected material after the explosion, the luminosity, temperature, mass, and the light curve of the nova eruption. The chemical composition of the ejecta can be observed through spectroscopy.

Photometry enables the measuring of luminosity, while the temperature can be determined by fitting a blackbody curve. The WD mass can be calculated through orbital mechanics or by analyzing the light curve in eclipsing binary systems. Continuous photometric monitoring can provide information regarding the light curve of the eruption. Once the mass of the WD is known other important properties affecting the TNR can be determined. For example, theoretical predictions suggest a compositional transition around 1.2–1.3 $M_\odot$, where CO WDs predominantly exist below this mass threshold, and ONe WDs are expected to exist within the mass threshold (Gehrz et al., 1998). The white dwarf's radius can be inferred through the mass-radius relation, which describes the radius as proportional to the mass of the WD via: $R \propto M^{-1/3}$. While the envelope mass can be calculated through the critical pressure needed to ignite the TNR, it is given by:

$$P_{\rm crit} = \frac{GM_{\rm WD}M_{\rm env}}{4\pi R_{\rm WD}^4} \tag{1.1}$$

where $P_{\rm crit}$ is the critical pressure needed which is roughly 10^{20} dynes cm^{-2}, G is the gravitational constant, $M_{\rm WD}$ is the mass of the WD, $M_{\rm env}$ is the mass of the accreted envelope and $R_{\rm WD}$ is the Radius of the WD.

Not all nova systems present uniform observables. In some cases, the WD may not be observed before the nova due to low luminosity during the accretion phase, or obscuration by the accretion disk. The WD may also be hidden after the explosion by the ejected material. Therefore, there may be some novae in which the WD is not directly observable, but the explosion properties, such as the light curve and the composition of the ejecta, are. However, if the WD can be observed before and after the explosion, it would provide valuable information about the properties of the binary system. These properties may be the mass of the companion star or the orbital period, which would indicate the type of mass transfer occurring. Additionally, comparing data from before and after the explosion would offer insight into how the explosion affects the binary system and the properties of both stars.

For the purposes of this work, however, the most important observable is the composition of the ejected material. The process of extracting chemical abundances from spectra of novae is complex, with each step involving its own uncertainties. Generally, model atmospheres are used to generate a nova spectrum that is compared with observations. In this model atmosphere, equations of radiative transfer must be solved, usually under the assumption of local thermodynamic equilibrium (LTE), while a non-LTE model is preferable. The abundances of elements from model spectra can be determined by using line ratios, meaning that emission line fluxes for one element are compared to the emission line fluxes of other elements.

Ca abundances in novae are determined using coronal lines, which are emission lines from highly ionized atoms. The observed spectral lines are formed in the expanding ejecta but can inform us of the nucleosynthesis that took place at the base of the accreted envelope on the surface of the WD. Fig. 1.4 contains a spectrum that was observed from the nova V977 Sco during the nebular phase; it contains spectral lines for many elements but notably for Ca and Ar. The nebular phase of classical novae typically occurs weeks to months after the initial eruption and is when the ejected material becomes optically thin, which allows radiation from the central WD to ionize the surrounding gas. As seen in Fig. 1.4, there are spectral lines for [Ca V] and [Ar II]; this notation indicates that Ca has been quadruply ionized, meaning that it has lost four electrons, and Ar has been singly ionized, meaning it lost one electron. For Ca to have lost four electrons it must be ionized by very high energy photons.

There are several sources of uncertainty in the derived abundances. One of which is the use of model atmospheres, which require assumptions about electron temperature and density. Additionally, each author may interpret the models, codes, and resulting spectra differently, leading to variability in the reported abundances, especially in older nova studies where uncertainties in the abundances are often not fully reported. Uncertainties in atomic data, potential line blending in the spectra, and limitations in spectral resolution can also contribute to the difficulty in accurately determining abundances.

For this work, observations of novae that date back 65 years have been collected and tabulated. A detailed review of the observations used in this research is given in Chapter 2.

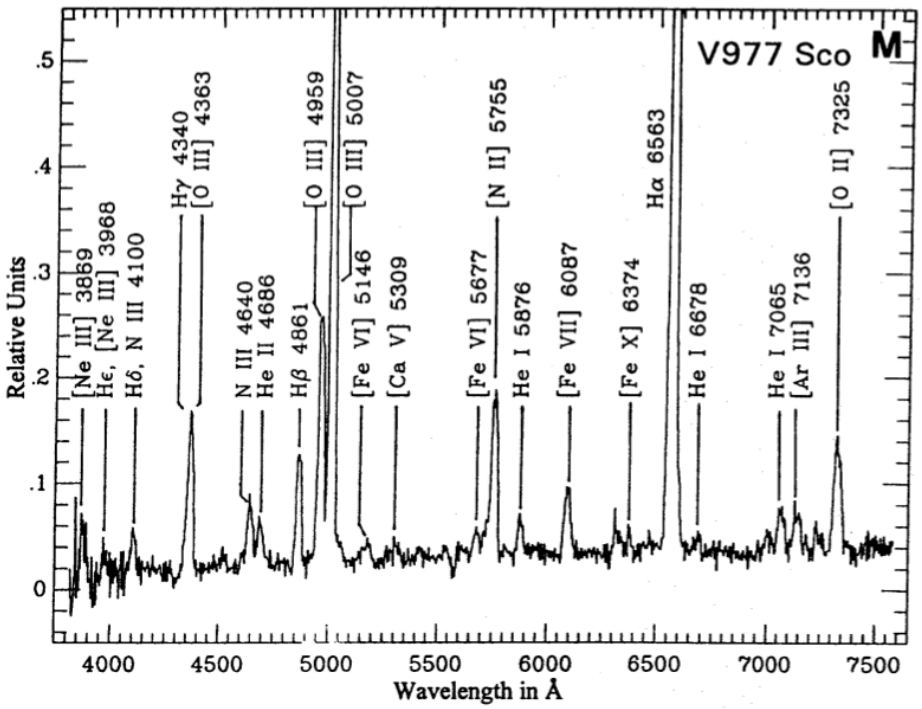

Figure 1.4: Optical spectra taken during the nebular phase from Nova V977 Sco. Image taken from Andrea et al. (1994).

1.3 Thermonuclear Reaction Rates

Thermonuclear reactions are nuclear reactions that depend sensitively on temperature. The rates at which these reactions occur are key inputs for stellar evolution and nucleosynthesis calculations. Classically, for a charged particle to be captured by a nucleus, the particle must have enough kinetic energy to penetrate the Coulomb barrier of the nucleus. However, quantum mechanics allows the particle to penetrate the barrier through quantum tunneling, even at low energies, albeit with a reduced probability. This thesis focuses on charged particle reactions involving the capture of protons and α particles as these are the dominant reactions relevant to novae nucleosynthesis.

The total reaction rate for particle interactions of non-identical nuclei, particles 0 and 1 for example, can be written in a general form:

$$r_{01} = \frac{N_0 N_1 \langle \sigma v \rangle_{01}}{(1 + \delta_{01})} \tag{1.2}$$

where N_0 and N_1 are the number density or the number of particles per cubic centimeter for a certain species. The number density can be written in two ways; the first using mass

fraction:

$$N = \rho\, N_A\, \frac{X}{A}. \tag{1.3}$$

Here, N_A is Avogadro's number, ρ is the density in units of g/cm^3, X is the total mass fraction summed over all isotopes for a given element, and A is the atomic mass number. The number density can also be written in terms of moles, with Y being the mole fraction of a given species:

$$N = \rho\, N_A\, Y. \tag{1.4}$$

The denominator in Equation 1.2 $(1 + \delta_{01})$, prevents double counting if the two particles are the same. The most important term is the $\langle \sigma v \rangle_{01}$ term which describes the probability of this reaction occurring as a function of cross-section and velocity. The $\langle \sigma v \rangle_{01}$ term can be calculated as follows,

$$\langle \sigma v \rangle_{01} = \int_0^\infty v P(v) \sigma(v)\, dv = \int_0^\infty v \sigma(E) P(E)\, dE = \left(\frac{8}{\pi \mu_{01}}\right)^{1/2} \frac{1}{(kT)^{3/2}} \int_0^\infty E \sigma(E) e^{-E/kT}\, dE. \tag{1.5}$$

where μ_{01} is the reduced mass of the particles, k is the Boltzmann constant, T is the temperature, and E is the center-of-mass energy. This term can be expressed in terms of velocity or center of mass energy by using the relation, $E = \frac{1}{2}\mu_{01} v^2$. The energy dependence of the cross-section will be discussed later in Section 1.3.3 in the context of resonances in nuclear reactions.

How quickly the reactions take place directly influences the nuclear timescale for novae. The two main nuclear timescales relevant to nova nucleosynthesis are the time it takes for a nucleus to capture a proton ($\tau_{(p,\gamma)}$) and the time it takes the nucleus to β^+ decay (τ_{β^+}). At lower temperatures and in equilibrium, the time it takes an isotope in the CNO cycle to decay is faster than the time it takes to capture a proton. However, as the temperature increases, the time it takes to capture a proton decreases and becomes faster than the β decays, allowing for breakout in the hot CNO cycle, or for captures on existing nuclei heavier than ^{20}Ne, which can lead to the formation of heavy elements.

The nuclear time scales for nova nucleosynthesis span several orders of magnitude, from millisecond-scale processes to radioactive decays lasting days to indefinite periods for stable isotopes. Charged particle reaction time scales are dependent upon specific nuclear interaction parameters such as nucleon configuration and spins and can range from milliseconds

to seconds. The reaction time scales determine the nuclear pathways that directly influence the composition of the ejecta. The balance between nuclear reaction rates and decay times determines the final abundances of synthesized isotopes, which are observed in the spectra of the ejecta.

1.3.1 Nuclear Reaction Networks

Nuclear reaction networks are essential for detailed calculations of nucleosynthesis using post-processing simulations of stellar evolution. Nuclear reaction networks consist of a number of coupled first-order ordinary differential equations (ODEs). The number of ODEs is proportional to the number of reactions taking place. The time evolution of a given nuclei, N_m, can be described by this equation taken from Herwig (2013).

$$\frac{dN_m}{dt} = N_k N_l \langle \sigma v \rangle_{kl,m} - N_m N_n \langle \sigma v \rangle_{mn,o} + \cdots + N_i \lambda_{i,m} - N_j \lambda_{m,j}. \tag{1.6}$$

where the production of said nuclei is contained in the first term, $N_k N_l \langle \sigma v \rangle_{kl,m}$, and the destruction of said nuclei is contained in the second term, $N_m N_n \langle \sigma v \rangle_{mn,o}$. Of course, there are multiple production and destruction channels, so this would be repeated for each channel with the general description given by the last term.

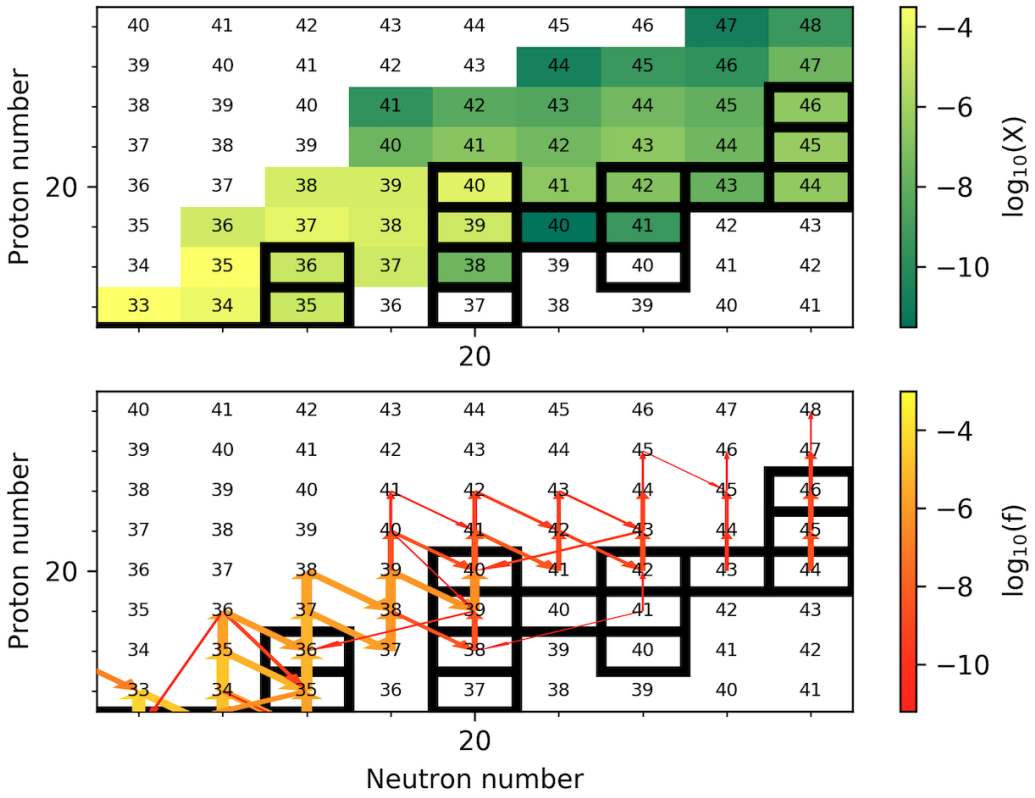

Figure 1.5: The mass fractions (upper panel) and reaction fluxes (bottom panel) in the region around ^{40}Ca for a single-zone simulation of an extreme nova model (see Chapter 2 for more details on the nova models). The snapshot shown here is for the cycle with the hottest temperature which is 4.04×10^8K. Boxes outlined in black are the stable nuclei.

Fig. 1.5 shows the mass fractions and reaction fluxes for isotopes in the region around ^{40}Ca for a single-zone simulation of an extreme nova model. The thickness and color of the arrows indicate the amount of reaction flux and the direction of the arrow indicates the direction of flux. Charts like these are useful for visualizing the different nuclear pathways that occur. Specifically, it can be seen that while ^{37}Ar contributes strongly to the production of ^{38}K through proton capture, ^{38}K is simultaneously being destroyed by the β^+ decay to ^{38}Ar and the proton capture to ^{39}K. This gives the reader an idea of the complexity of these nuclear reaction networks that are needed to understand the nucleosynthesis in these explosions.

1.3.2 Cross Section Measurements

The cross-section, σ, quantifies the probability of a given nuclear reaction occurring and is crucial in determining the reaction rate, as shown in Equation 1.5. While reaction rates can

be theoretically predicted, it is essential to also determine these rates experimentally. The reason for this is that nuclear theory and statistical models can only go so far. Predicting nuclear cross-sections is difficult because of the complexity of nuclear interactions and the use of approximate models. By directly measuring the cross-section experimentally, the need to calculate complex quantities is reduced. For example, the spectroscopic factor, which accounts for the spins of the interacting nuclei is inherently included in the experimental measurement. For all nuclei, at higher energies, the nuclear level density increases, meaning there are many closely spaced excitation levels. In a mass regime with a large Q-value, the interacting nuclei are close to multiple excitation levels which makes a statistical approach appropriate for calculating the cross section and therefore the reaction rate. However, in a low-mass regime, the Q-value decreases, especially for nuclei far from the valley of stability. For these low-mass, unstable isotopes, using a statistical model would not work, again highlighting the need for experimental measurements.

The cross-section can be determined experimentally through either inverse kinematics, where a heavy particle beam is accelerated towards a light target like H gas, or forward kinematics, where a heavy target is bombarded by a light particle beam, typically protons. In both cases, these experiments measure the cross-section for the reaction based on the definition provided by Iliadis (2015):

$$\sigma \equiv \frac{\text{(number of interactions per time)}}{\text{(number of incident particles per area per time)} \times \text{(number of target nuclei within the beam)}} \tag{1.7}$$

All of the above quantities can be determined experimentally thereby providing a value for the cross-section at a specific energy which can then be used to calculate the reaction rate. Many nuclear reactions are key to understanding nova nucleosynthesis and improving our models, and many of these have been experimentally measured. Rather than discussing all of them, I will highlight some recent measurements and their significance to the field.

The ^{22}Ne$(p,\gamma)^{23}$Na reaction is important in the Ne–Na cycle of H-burning, which occurs in classical novae. Uncertainties in this rate were found to significantly impact the abundances for isotopes around Ne Iliadis et al. (2002). To better constrain this rate, Williams et al. (2020) performed the first inverse kinematics measurement of this rate using the Detector of Recoils And Gammas Of Nuclear reactions (DRAGON) facility at TRIUMF. Recently, there has been a re-evaluation of the reaction rate using indirect methods Ali et al. (2024). The authors found that at temperatures relevant to hot bottom burning in AGB stars the reaction rate was 15% higher than the rate from Williams et al. (2020) but found no change to the reaction rate at temperatures relevant to classical nova. Since this rate is now well-

constrained experimentally, it can be incorporated into nova models.

Classical novae have been discussed as potential sources for presolar grains due to their unique isotopic abundance patterns (José & Hernanz, 2007b). However, a method of distinguishing grains that originate in novae from those that originate in supernovae is needed. ^{29}Si has been proposed as a potential diagnostic tool and recently, Downen et al. (2022) used direct measurement techniques to measure the ^{29}Si$(p,\gamma)^{30}$P reaction, which is the main sink for the ^{29}Si abundance in novae. The experimental results presented in this paper differed by up to 50% from previous results in the temperature range relevant to nova nucleosynthesis. The authors conclude that ^{29}Si can be used as a diagnostic for presolar grains originating from novae.

There are two radionuclides of particular interest to classical novae, ^{22}Na and ^{26}Al. When these isotopes decay, they emit gamma rays of specific energies, namely 1.275 MeV and 1.809 MeV, making them potential observables. Since these isotopes are synthesized in novae and then ejected into the interstellar medium, novae may contribute to the galactic abundance of these elements. However, the amount produced in novae depends on the reaction rates for the production and destruction of these isotopes, which can be uncertain. To better constrain these rates, Sallaska et al. (2010) measured low energy resonances that contribute to the overall reaction ^{22}Na$(p,\gamma)^{23}$Mg rate and found that ^{22}Na in novae is destroyed much more efficiently than previously thought. Additionally, Ruiz et al. (2006) measured the strength of a resonance in the ^{26}Al$(p,\gamma)^{27}$Si reaction and found that the overall reaction rate should be lower, favoring the production of ^{26}Al. When this new rate was tested on a nova model the authors found that the abundance of ^{26}Al increased by 20%.

These experimental measurements highlight the interdependence between nuclear physics, computational modeling, and observational astrophysics.

1.3.3 Nuclear Physics Uncertainties

One of the main goals of this work is to investigate the impact of nuclear physics uncertainties on the production of Ca in nova models. The largest area of nuclear physics uncertainties relevant to nova nucleosynthesis lies in the reaction rates. Other processes, such as the nucleosynthesis from the rapid neutron capture process, are impacted more strongly by the uncertainties in the masses of nuclei than their reaction rates (Mumpower et al., 2024).

As previously shown in Equation 1.5, the likelihood that a reaction will occur depends on the energy. Resonant reactions occur when the sum of two energies, namely the relative kinetic energy of the interacting particles and the reaction Q-value, matches exactly with an

excited state energy level in the temporary combined nuclear system, otherwise known as the compound nucleus. At these specific energies, the probability of nuclear interaction increases dramatically, leading to a sharp peak in the reaction cross section as seen in Fig. 1.6. The frequency of these resonances over a given energy range depends on how closely spaced the energy levels are in the compound nucleus.

Furthermore, there could be several resonances that contribute to the total reaction rate for a given reaction. The total reaction rate is calculated by summing the contributions from each individual resonance, taking into account their respective strengths and energies. For example, Longland & de Séréville (2020) found that accounting for resonance energy correlations is important for reaction rate calculations involving unstable nuclei, where resonance energies have large, correlated uncertainties due to uncertain reaction Q-values.

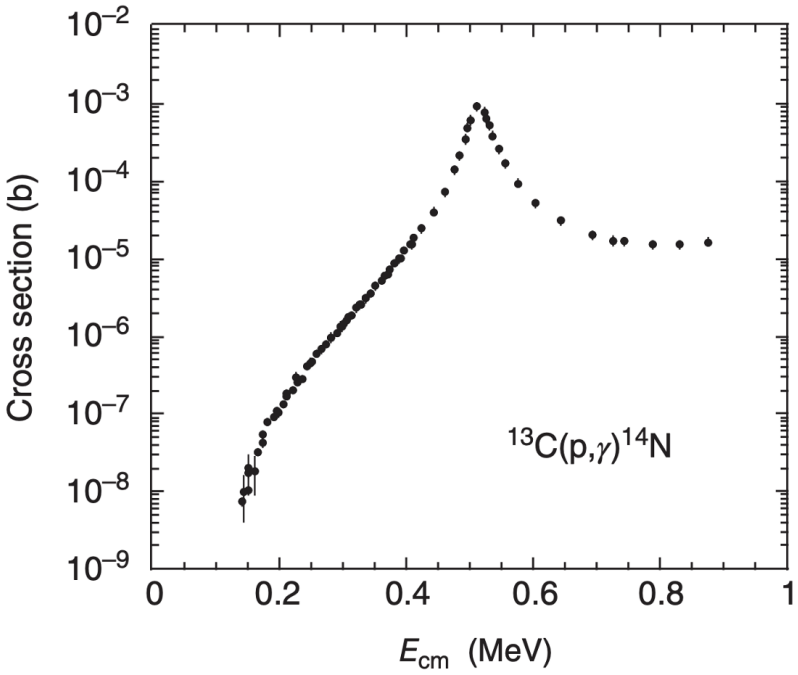

Figure 1.6: Schematic of resonance in the $^{13}C(p,\gamma)^{14}N$ reaction (Iliadis, 2015).

The level density and Q-value are well-known for most reactions involving lighter nuclei, as they have been determined experimentally. For heavy nuclei where the level density is high, meaning there are many energy levels for a given nucleus, it is appropriate to calculate the reaction rate and associated uncertainties with a statistical model like Hauser-Feschbach (Denissenkov et al., 2021a). However, for the region around Ca the level densities for these nuclei are less well known, and using a statistical model would not work because the reaction

rate is dominated by a few individual, isolated, or narrow resonances that increase the probability of the reaction happening, thus causing the overall reaction rate to be uncertain by a factor of 10 or even 100.

1.4 Computational Nuclear Astrophysics

1.4.1 Stellar Structure Equations

There are a set of differential equations that govern how stars evolve during their lifetime. These equations are often written in terms of the stellar radius; however, for stellar modeling, it is more useful to write these equations in terms of mass, i.e. in Lagrangian form (Kippenhahn et al., 2013).

The first equation is the equation of hydrostatic equilibrium, which describes the balance between gravitational forces and pressure forces. Most stars spend the majority of their lifetimes in this state of equilibrium. This equation assumes spherical symmetry and no rotation. To consider the effects of rotation, one would have to add an additional term to this equation.

$$\frac{\partial P}{\partial m} = -\frac{Gm}{4\pi r^4} \tag{1.8}$$

Here P is the pressure, G is the gravitational constant, m is the enclosed mass, and r is the radius.

The second equation is the mass continuity equation, which describes the sum of the masses of infinitesimally thin spherical shells as equaling the total mass of the star. This formula assumes there is no mass loss and an additional term would have to be added to take this into account.

$$\frac{\partial r}{\partial m} = \frac{1}{4\pi r^2 \rho} \tag{1.9}$$

Here, ρ is the density.

The third equation describes the mode of energy transport in the star, which depends on whether the region is in a convective or radiative regime meaning whether things are transported through radiation or convection.

$$\frac{\partial T}{\partial m} = \begin{cases} \nabla_{\text{rad}} = -\frac{3}{64\pi^2 ac}\frac{\kappa l}{r^4 T^3}, & \text{for radiative transport} \\ -\frac{GmT}{4\pi r^4 P}\nabla_{\text{ad}}, & \text{for convective transport} \end{cases} \tag{1.10}$$

Here, T is the temperature, κ is the opacity, a is the radiation constant, and c is the speed of light. For convective transport, $\nabla_{\rm ad}$ represents the adiabatic temperature gradient. The process that occurs depends on which temperature gradient is smaller, convective or radiative. If $\nabla_{\rm rad} < \nabla_{\rm ad}$, the region will be stable against convection. However, if $\nabla_{\rm ad}$ is smaller than the radiative temperature gradient, the region will become convectively unstable, and convection will occur.

The fourth equation describes energy conservation within the star, where energy sources and sinks are summed to determine the total energy. For example, energy is generated through nuclear reactions, while it is lost through processes such as neutrino emission and changes in the star due to expansion or contraction.

$$\frac{\partial L_r}{\partial M_r} = \sum_i \epsilon_i \tag{1.11}$$

While these equations guide the modeling of stellar interiors, the microphysics, which details the properties of the stellar matter should also be included. The equation of state (EOS), the opacity of the material, the thermonuclear reaction rates, and the nuclear reaction networks all need to be considered when modeling stars.

1.4.2 Historical Nova Models

As discussed, novae are complex three-dimensional hydrodynamic events which makes modeling them quite challenging. Classical novae have been modeled extensively throughout history. Below I will highlight some impactful previous works.

Giannone & Weigert (1967) conducted some of the first hydrostatic simulations of nova outbursts showing that a TNR resembling a nova-like event can be driven by accretion onto a white dwarf. The study by Starrfield et al. (1971) was among the first to present results from a hydrodynamic nova model. The authors used a one-dimensional hydrodynamic code coupled with a nuclear reaction network. Shortly after, Prialnik & Kovetz (1995) simulated the long-term evolution of novae through multiple outburst cycles, rather than just a single eruption. State-of-the-art one-dimensional hydrodynamic models with extensive nuclear networks were developed by José & Hernanz (1998); Starrfield et al. (1998) providing detailed nucleosynthesis predictions for a wide range of nova parameters. Most recently, José et al. (2020) introduced a novel "123-321" approach for modeling classical nova outbursts, combining 1D and 3D simulations. Their method uses 1D modeling for the early stages, then transitions to 3D when convection becomes extensive, and finally feeds key 3D-derived

parameters back into the 1D code to complete the simulation. This approach, which captures the effects of 3D turbulent convection, yields results that better align with observations compared to traditional 1D models.

These models set a new standard in the field, offering comprehensive comparisons with observations and insights into the role of novae in galactic chemical evolution. The computational approach to nova studies has since expanded to include multidimensional simulations and detailed explorations of nuclear reaction rate uncertainties, continually refining our understanding of these fascinating stellar explosions.

1.4.3 Models for This Work

For the work presented in this thesis, the Nova Framework (Denissenkov et al., 2014) was used to create single and multi-zone models of CO and ONe novae for five different combinations of WD mass, central temperature, and accretion rate. For more detail on the model parameters see Chapter 2. The Nova Framework works by decoupling the stellar structure and nucleosynthesis and solves them separately. The one-dimensional stellar evolution of these models was calculated using the Modules for Experiments in Stellar Astrophysics code (`MESA`) Paxton et al. (2011, 2013), which is embedded in the Nova Framework. The nucleosynthesis was post-processed using codes from NuGrid (Herwig et al., 2008), which is also embedded in the Nova Framework.

`MESA` has all the capabilities needed to model classical novae, as it implicitly and numerically solves the nuclear and stellar structure equations simultaneously. This allows `MESA` to model key novae components such as accretion, mass loss, and the TNR. It handles microphysics through dedicated modules for different aspects. For example, `MESA` uses precomputed tables that provide values like pressure and internal energy for given temperatures and densities. Similarly, for opacities, `MESA` relies on tables that contain values based on temperature, density, and composition. Nuclear reaction rates are derived from libraries such as NACRE and REACLIB which provide temperature-dependent rates. `MESA` solves the stellar structure equations over time to track stellar evolution, using a limited nuclear network to compute energy generation from nuclear fusion. The inputs needed to run `MESA` within the Nova Framework are the WD mass, initial chemical composition, central temperature, and the accretion rate. Additionally, the chemical composition of the accreted envelope is provided before running the simulations.

The outputs of `MESA` are files that contain the stellar properties of a star at each timestep. In other words, the `MESA` outputs are time-dependent profiles that resolve the WD and

envelope into mass zones, allowing MPPNP to model mixing and transport between layers or allowing SPPN to follow a single mass coordinate. These outputs are then used as inputs for the Post-Processing Nucleosynthesis calculations (PPN) that are used to understand the detailed nucleosynthesis that takes place; this involves a more detailed nuclear network than the one used in MESA. The nucleosynthesis needs to be post-processed because it would be too computationally expensive to include alongside the hydrodynamics, so it is calculated separately from the stellar evolution.

To do the post-processing the Single-zone Post-Processing Nucleosynthesis (SPPN) code and the Multi-zone Post-Processing Nucleosynthesis Parallel (MPPNP) code from the NuGrid collaboration are used. For the post-processing calculations, the initial inputs are the stellar structure and evolution information, isotope selection, and reaction rate networks (e.g., JINA REACLIB, NACRE). The SPPN code works by taking a temperature and density trajectory that has been extracted from the stellar evolution as input. This trajectory is time-dependent with no spatial coordinates and assumes a uniform temperature and density throughout the envelope. Importantly, this means that time-dependent mixing is not taken into account. SPPN solves the nuclear network that contains all the ODEs for nuclear reactions taking place. The outputs of SPPN are files that contain detailed elemental and isotopic abundances. SPPN is computationally inexpensive, quick, and easy to learn, making it ideal for qualitative investigations of nuclei.

The full profiles from MESA that get used by MPPNP split the WD and the accreted envelope into mass zones. These mass zones are thin shells within the WD or the accreted envelope characterized by temperature, density, pressure, and composition. They are defined by the total enclosed mass with more zones near the base of the accreted envelope. MESA uses adaptive mesh refinement to dynamically adjust the number and size of zones during the simulation to ensure numerical accuracy. MPPNP works by treating the different mass zones as distinct computational shells, each with its own set of nuclear abundances and properties. The nuclear network is solved independently within each zone, assuming no mixing. Once the reactions are computed, the resulting abundances are then mixed using the diffusion coefficient from MESA .

The output of MPPNP simulations contains full stellar structure profiles such as temperature, density, and pressure, as well as detailed chemical abundances of elements and isotopes, which are mass-averaged across the entire envelope. By mass averaging over all zones in the last time step, a single data point for the abundance of a given isotope is obtained, assuming that all zones in the expanding envelope will be ejected (Denissenkov et al., 2014). MPPNP employs an operator-split approach, solving the nuclear networks and the mixing and trans-

port of materials between different zones separately. This makes MPPNP more computationally expensive but also more realistic compared to single-zone simulations.

Table 1.1 summarizes the differences between these two post-processing methods. As will be shown later in Chapter 2, the key reactions identified by the Monte Carlo (MC) simulations differ slightly between SPPN and MPPNP .

Aspect	PPN**(Single-Zone)**	MPPNP **(Multi-Zone)**
Dimensionality	No spatial dimension	1D spatial dimension
Mixing Processes	Not included	Included (convection, diffusion, etc.)
Complexity	Simpler Less computationally intensive	More complex Computationally demanding
Applications	Specific scenarios Parametric studies	Stellar evolution Detailed nucleosynthesis studies
Input Requirements	Initial abundances T and ρ trajectories	Stellar profiles Mixing coefficients
Numerical Methods	Solves ODEs for nuclear reactions	Solves ODEs and PDEs Uses operator splitting
Flexibility	High flexibility Easy customization	Complex customization

Table 1.1: Key differences between the single-zone and multi-zone post-processing nucleosynthesis simulations from NuGrid.

1.4.4 Monte Carlo Simulations

MC simulations are a computational technique used to better understand uncertainties in complex systems. MC simulations use random sampling to understand the possible outcomes of complex systems, like classical novae.

One of the first MC simulations to investigate the impact of nuclear physics uncertainties on nova nucleosynthesis was performed by Hix et al. (2003). The authors used a single-zone post-processing nova simulation, similar to the SPPN models used in this work, to perform MC simulations on a 1.25 ONeMg WD. They found that uncertainties in the nuclear reaction rates can lead to variations in the abundances of key isotopes like ^{22}Na and ^{26}Al by factors of 2–4 and over 2 orders of magnitude for ^{7}Be. Their work highlighted how nuclear physics uncertainties limit the reliability of nova nucleosynthesis simulations especially in

the context of comparing with observations, and advocated for these reaction rates to be better constrained through experimental nuclear physics. As well, Iliadis et al. (2002) performed a sensitivity study that varied the rates of individual reactions for hydrodynamic nova models to also investigate the impact of nuclear physics uncertainties. They varied 175 reactions individually and then analyzed the impact on abundance for 142 isotopes. They found that nova simulations were able to predict reliable abundances for lighter elements such as Li, Be, C, and N given the nuclear physics uncertainties. Conversely, the nuclear physics uncertainties had a large impact on the abundance of heavier elements such as O, F, Ne, Na, Mg, Al, Si, S, Cl, and Ar and would need to be further constrained to be reliable. Both of these previous works demonstrated the importance of better constraining nuclear rates for improving nova nucleosynthesis models. The Monte Carlo approach of Hix et al. (2003) provides a global view of uncertainties, while the systematic variations of Iliadis et al. (2002) pinpoint specific influential rates.

In this research, MC simulations are also performed for `SPPN` simulations of novae. Unlike the previous works, however, the research presented in this thesis is novel in that for the first time MC simulations were performed on multi-zone nova models. The results of this will be discussed in more detail in Chapter 2.

1.4.5 Accuracy, Assumptions, and Approximations

Classical novae are complex 3D hydrodynamic explosions but more often than not they are treated as 1D and the hydrodynamic aspects are excluded. Modeling stellar evolution, nucleosynthesis, and hydrodynamics individually is computationally advanced but to model all simultaneously is incredibly challenging and computationally expensive. To accommodate this, assumptions and approximations are used to model specific aspects of these events. Below the main assumptions and approximations of tools used to complete this project are discussed.

Firstly, the `MESA` and NuGrid simulations all treat the problem as one-dimensional. As well, it is assumed that the nova is spherically symmetric, which means any angular variations in temperature, density, or pressure are not accounted for. However, in reality, the explosion is likely asymmetrical. The assumption of spherical symmetry also neglects hydrodynamic instabilities, such as Kelvin-Helmholtz and Rayleigh-Taylor instabilities, which cannot be directly modeled in 1D simulations. Instead, diffusion or mixing-length approximations are used to account for mixing processes.

Since `MESA` is used to compute the stellar evolution and then `MPPNP` is used for the

nucleosynthesis calculations, any energy generation from nucleosynthesis is not fed back into the stellar structure. However, this is only a problem when the nucleosynthesis processes significantly alter the star's structure during the timescale of interest for example, in core-collapse supernovae. Usually, the nuclear network used to compute the stellar evolution is selected such that it only includes the isotopes that have the greatest impact on energy generation. For these reasons, this approximation is acceptable for nova models.

`MESA` can account for some hydrodynamics, for example, the mixing between the WD and accreted material through convective boundary mixing (CBM) which is the result of hydrodynamic instabilities and shear-flow turbulence as a result of steep horizontal velocity gradients (Casanova et al., 2010, 2011). In `MESA` that is used in the Nova Framework, this mixing is treated as a diffusive process. While this method is more reflective of the actual physics taking place, it is of course computationally expensive. Instead, an approximation can be made; assume the accreted material is pre-mixed with a composition of 50% solar material and 50% WD material. Denissenkov et al. (2014) showed that this approximation yields similar peak TNR temperatures for nova models and thus is valid.

When it comes to modeling novae, the largest flaw of `MESA` is that it cannot account for the dynamics of the explosion and can only model the mass loss and material ejected after. In order to fully model the explosion one would need to use a multi-dimensional hydrodynamic code.

Despite the assumptions and approximations discussed, these models remain a valuable tool for understanding stellar nucleosynthesis. While the dynamics of the explosion cannot be well captured, these 1D models still reproduce key observables, such as the light curves and nucleosynthetic yields. As briefly mentioned earlier, one of the largest sources of uncertainty in these models stems from nuclear physics inputs. By evaluating the impact of nuclear physics uncertainties on nova models, this thesis demonstrates how such models can be further tested and constrained.

1.5 Outline

The outline for the rest of this thesis is structured as follows. Chapter 2 presents the manuscript on which this thesis is based. A detailed discussion of the results presented in the manuscript are highlighted in Chapter 3. Finally, the results and implications of this research are discussed in Chapter 4.

Chapter 2

Calcium Excess in Novae: Beyond Nuclear Physics Uncertainties

The contents of this chapter are based on a paper that has been submitted to the Astrophysical Journal. The contributors to this paper are myself, Dr. Pavel Denissenkov (P.D.), Dr. Chris Ruiz, Dr. Falk Herwig, and Dr. Alan Shotter (A.S.). A detailed breakdown of their contributions is described below.

Conceptualization: C.R. conceived the original idea for this project, which heavily relies on a framework previously developed by P.D. Methodology: M.L. ran the MESA simulations for 5 nova models, performed the MPPNP and PPN simulations on the MESA models, and carried out Monte Carlo simulations on both the PPN and MPPNP models. Software: M.L. modified P.D.'s codes for analysis and wrote original code for comparison with observations. P.D. wrote the original code modified by M.L. and developed the foundational framework upon which this work is based. Validation: P.D., C.R., and F.H. provided feedback on the results and their interpretation. Formal analysis: M.L. conducted the formal analysis of the simulation results. Investigation: M.L. conducted the primary investigation by running simulations and analyzing the results. Resources: P.D. guided running the simulations. Data curation/collection: M.L. curated the data generated from the simulations and collected observational data through a literature search. Writing (original draft): M.L. wrote the majority of the paper. Writing (review & editing): P.D. contributed to the paper by adding a section about the CaNPAN project and providing clarifying sentences throughout. C.R. and F.H. provided feedback on the manuscript. Visualization: M.L. created visualizations of the data for the paper. Supervision: P.D., C.R., and F.H. provided supervision and guidance throughout the project. A.S. Provided insightful discussions for the dust fractionation scenario.

2.1 Introduction

Classical novae, understood as thermonuclear runaways (TNRs) of H burning on accreting white dwarfs (WDs) in close binary systems with a main sequence or evolved companion star, have been extensively modeled (e.g., Prialnik & Kovetz, 1995; José & Hernanz, 1998; Glasner & Truran, 2009; Denissenkov et al., 2014; Starrfield et al., 2021). They are one of the most frequently observed cataclysmic variables, with a few out of a predicted 20–70 eruptions per year observed in the Milky Way galaxy (Darnley et al., 2006; Shafter, 2017b). A vast amount of spectroscopic data exists for novae, but only a few spectroscopic measurements of elemental abundances around Ca have been made. Despite the generally accepted theoretical expectation that novae should not produce Ca, spectral observations of novae exist in which Ca abundance appears to be enhanced compared to its solar value (Andrea et al., 1994; Arkhipova et al., 2000; Evans et al., 2003; Morisset & Pequignot, 1996; Pottasch, 1959; Woodward et al., 2021). The overabundance of Ca in these novae could indicate observational errors, reveal limitations in our nova models, suggest issues with nuclear physics inputs, or point to gaps in our understanding of the nova environment. Moreover, as Ca represents the approximate termination point of nova nucleosynthesis, it serves as a test of our models and understanding of nucleosynthesis in novae. We have tabulated and compared observed abundances of Ca in novae with those from our nova models, along with abundances of other elements measured in the same novae, and conclude that indeed there is a puzzling large excess of Ca. We find a similar situation for Ar.

Observations of novae with estimated Ca abundances date back to 1959, when Pottasch (1959) determined temperatures and radii of central stars for six novae and reported abundances of elements heavier than H. Ca abundances in novae were reported again in 1994 when they were determined for 11 novae using UV and optical spectra (Andrea et al., 1994). The authors reported abundance uncertainties of factors 2–3, noting that collisionally excited lines are sensitive to assumed temperature and density inputs in their models. Shortly after, Morisset & Pequignot (1996) used photoionization models to report a Ca abundance in the nova GQ Mus. They estimated that Ca was overabundant by a factor of 3 compared to its solar abundance, but also stressed the importance of using accurate atomic data for reliable abundance measurements. Hydrodynamic models of nova nucleosynthesis published by José & Hernanz (1998) were shown to reproduce available abundance measurements up to Ne from nova spectroscopic observations quite well. Later, Arkhipova et al. (2000) reported abundances for the nova V705 Cas using UV spectra, where Ca was again shown to be overabundant compared to solar. However, the uncertainties in the line intensities were

approximately 20–30%, which were then propagated to large uncertainties in abundances.

The production of intermediate-mass elements in novae had been previously explored by José et al. (2001). They mentioned that some enhancements of heavier species, such as Ar, K, and, to some extent, Ca were obtained for an extreme nova model with the a high peak temperature. The synthesis of Ca was not described in depth there. In 2002, sensitivity studies and in 2003 single-zone Monte Carlo (MC) simulations for reaction rate uncertainty studies of nova nucleosynthesis were performed, respectively, by Iliadis et al. (2002) and Hix et al. (2003), in the first work, nuclear reaction rates were multiplied and divided by fixed factors one by one for 142 isotopes, and the impact of those changes on abundances calculated using one-zone nova trajectories was reported. In the second work, all reaction rates relevant to nova nucleosynthesis were randomly varied within their estimated uncertainty ranges, and the impact of those variations on predicted abundances was reported.

Evans et al. (2003) presented results of spectroscopic observations of the nova V7223 Cas, in which temperature and abundance ratios were estimated. In that paper, it was proposed that the overabundances of S and Ca observed in that nova might be associated with its more evolved companion star.

The abundance of ^{7}Be in novae is traditionally determined using the equivalent widths of ^{7}Be II and Ca II lines and the assumption that the ionization fractions of Be II/Be and Ca II/Ca are equal as shown by Chugai & Kudryashov (2020). The authors found that the ionization fraction of Be II/Be in the nova V5668 Sgr should be at least a factor of 10 higher than Ca II/Ca. The authors assumed that the Ca abundance in this nova envelope was solar because Ca is not synthesized in novae. Since the measurements of the ^{7}Be abundance in novae depend on the strength of Ca spectral lines, and if Ca abundances are really enhanced in some novae, this may impact estimates of observed values of the ^{7}Be abundance in novae, which have recently been reported to be too high compared to model predictions (Denissenkov et al., 2021b, and references therein).

In this paper, we investigate whether uncertainties in nuclear reaction rates activated during nova TNRs could account for the observed Ca overabundances. In Section 2.2 our nova models will be established as suitable and comprehensive for comparison to observations by verification with previously published results. Section 2.3 directly compares our nova models with observations and clearly shows the overabundance of Ca. The impact of nuclear physics uncertainties on Ca production and the identification of key reactions whose rate uncertainties are correlated with Ca production are discussed in Section 2.4. In Section 2.5, the results of different mixing scenarios are discussed. Alternative explanations for the observed overabundance of Ca are presented in Section 3.1. Finally, in Section 4.1, we summarize the

main findings of this work.

2.2 Nova models

For simulations of nova TNRs reaching different peak temperatures of H burning, we use the Nova Framework (Denissenkov et al., 2014) to create multi-zone models of Carbon-Oxygen (CO) and Oxygen-Neon (ONe) novae for five different combinations of WD mass, central temperature, and accretion rate (see Table 2.1 for a summary). These models are computed with revision 5329 of the stellar evolution code `MESA` embedded in the Nova Framework, now part of the CaNPAN computational tools[1]. We also use one-zone nova models with maximum temperature and density trajectories extracted from our more realistic multi-zone models. Elemental and isotopic abundances are computed using the NuGrid one-zone and multi-zone post-processing nucleosynthesis codes (Herwig et al., 2008; Pignatari et al., 2016). As mentioned in the introduction, observations of novae suggest that in some of them, Ca is overabundant compared to solar. Results of our post-processing nucleosynthesis computations for the multi-zone nova models are compared with observations in Section 2.3 to investigate this Ca abundance discrepancy. Nova models typically predict that the highest thermonuclear runaway (TNR) peak temperatures are achieved in systems with the most massive white dwarfs (WDs), as well as the lowest WD central temperatures and accretion rates (Glasner & Truran, 2009). Achieving the highest possible temperatures during the TNR maximizes the probability of Ca production. Nova Model 5 with a peak temperature of 4.04×10^8 K, hereafter referred to as our hottest multi-zone nova model, gives the highest likelihood of producing heavy elements, such as Ar, K, and Ca, during the nova explosion.

Table 2.1: WD type, mass, central temperature, accretion rate, and peak TNR temperature of our multi-zone nova models.

Nova Model	WD Type	$M_{WD}[M_{\odot}]$	$T_{WD}[10^6 K]$	$M_{acc}[M_{\odot}\,yr^{-1}]$	T_{max} $[10^6 K]$
1	CO	1.15	12	2×10^{-10}	232
2	CO	1.15	10	10^{-11}	253
3	ONe	1.15	12	2×10^{-10}	261
4	ONe	1.3	20	2×10^{-10}	321
5	ONe	1.3	7	10^{-11}	404

The Nova Framework (Denissenkov et al., 2014) involves using the stellar evolution code

[1] https://github.com/dpa1983/canpan_projects/blob/main/README.md

MESA (Paxton et al., 2011, 2013) and the multi-zone post-processing nucleosynthesis code of NuGrid (Herwig et al., 2008). The MESA revision 5329 code is used in the Nova Framework to compute the evolution of nova models during their accretion, explosion, and nova-envelope early expansion phases. The MESA output files with the temperature, density, radius, and diffusion coefficient profiles as functions of time and mass coordinate are then used in post-processing nucleosynthesis computations done with the NuGrid Multi-zone Post-Processing Nucleosynthesis Parallel code (MPPNP). The MESA output files are also used to extract one-zone maximum temperature and density trajectories for the corresponding multi-zone nova models that can be used for individual Single-zone Post-Processing Nucleosynthesis computations done with the NuGrid code (SPPN) as well as for one-zone MC simulations. To facilitate nova TNRs in the multi-zone nova models, we use the mixing prescription in which the accreted material represents a mixture of 50% solar-composition material from the companion star and 50% material from the outer layers of the accreting WD. The presence of such mixtures in novae is supported by the spectroscopic measurements of high metallicities in nova ejecta (Gehrz et al., 1998). In this work, the standard treatment for all models assumes a pre-mixed abundance distribution composed of 50% WD material and 50% solar composition material, based on Grevesse & Noels (1993) solar abundances. This pre-mixed composition is critical for accurately simulating the effects of mixing between the WD material and the accreted H-rich envelope in nova outbursts. Before accretion, the outermost layer of a WD is typically expected to consist of a thin hydrogen-rich shell remaining from its prior stellar evolution. It is assumed that the WD material that is mixed with the accreted envelope originates from beneath this H-rich surface and is enriched in heavy elements such as C, O, or Ne, depending on the WD type, which are incorporated into the accreted material. In our models, we assume that the H layer on the WD surface has been processed or burned off, simplifying the focus to the mixing of heavier elements from these deeper layers. Mixing between the WD material and the accreted hydrogen envelope is essential for reproducing observed nova light curves. Without mixing, energy generation during the TNR is limited by the β^+ decay times of short-lived isotopes such as ^{13}N, ^{14}O, ^{15}O, and ^{17}F. These isotopes have decay times on the order of minutes, with ^{13}N having the longest decay time of roughly 10 minutes. The nuclear energy generation rate is then determined by these decay times and convection. Convection transports ^{13}N away from the burning region at the base of the accreted envelope, where temperatures are insufficient for H-burning via the CNO cycle, preventing further proton capture on ^{13}N (Starrfield et al., 2016). This transport bottlenecks nuclear energy production at ^{13}N unless fresh ^{12}C and ^{16}O from the WD are mixed into the envelope for further proton captures. Without this replenishment, energy production is proportional to the abundance

of pre-existing CNO nuclei (Glasner & Truran, 2012). An illustration of this can be seen in Figure 6 of Denissenkov et al. (2013) where without the inclusion of mixing, the nova light curve is much flatter and rises more slowly which does not agree with the observations. Denissenkov et al. (2014) showed that the multi-zone nova models computed with this 50/50 mixing prescription produce final elemental abundances in expanding nova envelopes similar to those obtained for the same models, but with mixing between the WD core and accreted solar-composition material modeled as exponential convective overshooting with the e-folding length scale $f = 0.004$ of the pressure scale height.

The nova models presented by José & Hernanz (1998), hereafter referred to as the Barcelona Group, have parameters similar to ours. Their models show good agreement with observations of elemental abundances in various novae for lighter-mass elements: from H to Ne. In this work, we are interested in the synthesis of elements near and up to Ca; therefore, we compare our results to theirs for elements beyond Ne in Fig. 2.1. The models presented in this work show good agreement with those from the Barcelona group. Any discrepancies are likely to be caused by updated reaction rates in our network, slightly different initial chemical compositions of the accreted mixture (see Fig. 4 of Denissenkov et al., 2014), and differences in the maximum WD masses. For example, model ONe6 of the Barcelona Group has a WD mass of 1.35 $M_\odot$, which is closer to the Chandrasekhar mass limit for WDs than the maximum WD mass of 1.3 $M_\odot$of our ONe nova models. Given that the results from the Barcelona Group demonstrated good agreement with observations of lighter mass elements in novae, and the comparison of our nova models with theirs shows good agreement for heavier elements, we can infer that nova models can be reliably compared to observations. Therefore, it is now possible to directly compare our models with the observations of Ca abundances in novae.

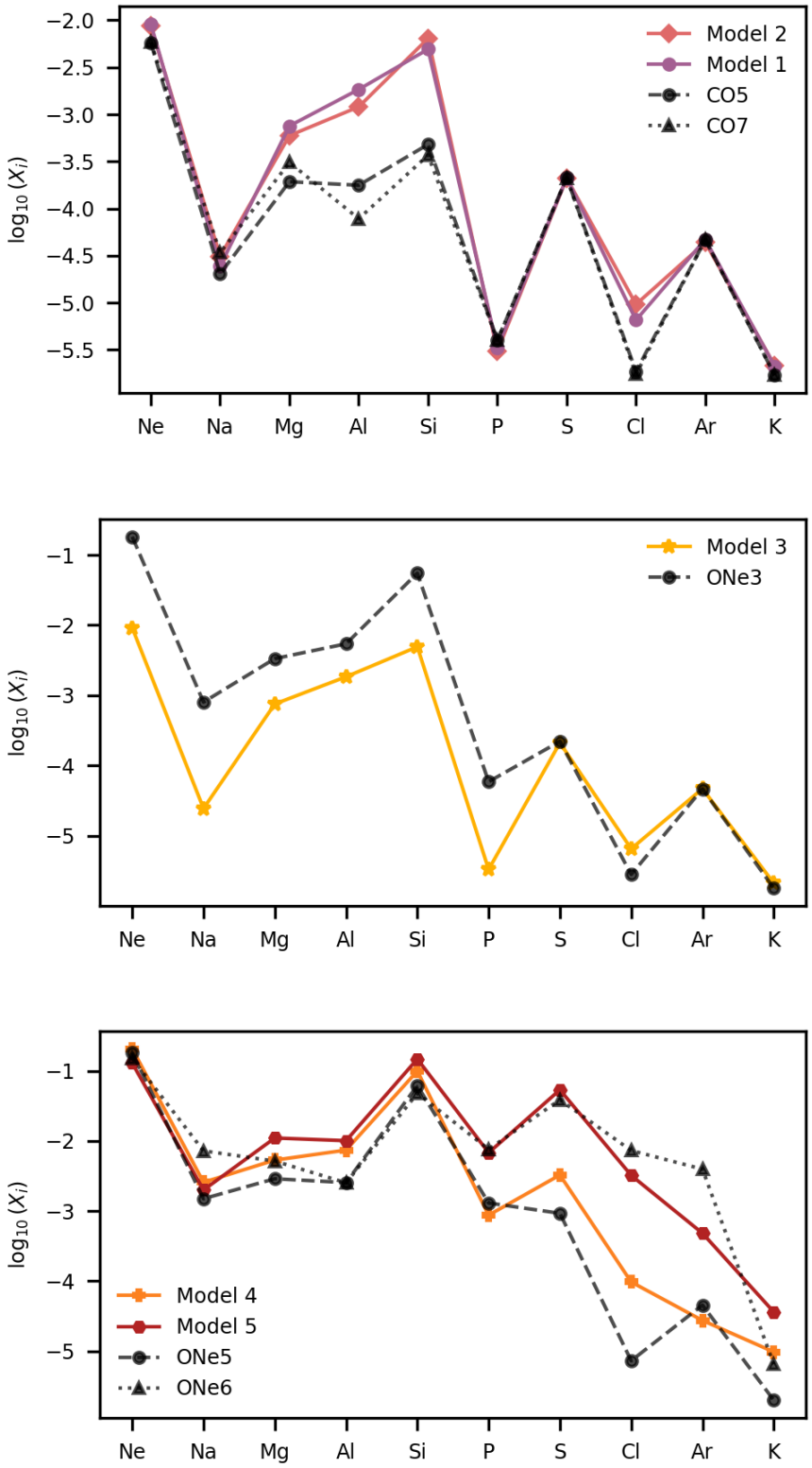

Figure 2.1: Comparison of elemental mass fractions from our multi-zone nova models (`MESA` and `MPPNP` simulations in the Nova Framework, solid-color lines) with those of the Barcelona Group (black dashed and dotted lines). Models selected from the Barcelona group have parameters closest to ours for both CO and ONe novae (José & Hernanz, 1998).

2.3 Comparison with observations

It has previously been mentioned that the abundances of Ca observed in some nova ejecta appear to be enhanced. We have gathered observational data for novae with measured Ca abundances, some of which are reported in mass fractions, and others in number densities. For more details on the observational abundances, see Table A.1 in the appendix. Abundances from our nova models are presented in mass fractions averaged over their entire expanding envelopes. Therefore, the observed elemental abundances that are reported in number densities need first to be transformed to their corresponding mass fractions. The observed number densities are usually reported as ratios with respect to some other element, like

$$\left(\frac{N_{\rm Ca}}{N_{\rm H}}\right) \text{ or } \left(\frac{N_{\rm Ca}}{N_{\rm Si}}\right). \tag{2.1}$$

The number density of an element i is related to its mass fraction as

$$N_i \approx \frac{X_i \rho N_{\rm A}}{A_i}, \tag{2.2}$$

where ρ is the mass density, $N_{\rm A}$ is Avogadro's number, and A_i is the atomic mass of the element. The atomic masses used in these calculations are assumed to be the average atomic masses of stable isotopes with their terrestrial relative abundances. Hence, the ratio of mass fractions for two elements can be written as

$$\frac{X_{\rm Ca}}{X_{\rm H}} = \frac{N_{\rm Ca} A_{\rm Ca}}{N_{\rm H} A_{\rm H}} \tag{2.3}$$

To see how overabundant the elements are compared to solar we compare abundances from our models and the observations in the standard stellar spectroscopy bracket notation $[X_{\rm i}/X_{\rm H}]$. Abundances from nova simulations are typically reported as elemental or isotopic mass fractions relative to solar values (José & Hernanz, 1998), while isotopic abundances are used for investigation of pre-solar grains of purported nova origin (Amari et al., 2001). However, calculating $X_{\rm i}/X_{\rm i,M_\odot}$ from ratios of number densities requires us to assume the abundance of H in the nova ejecta, which varies from star to star and is difficult to measure observationally (Gehrz et al., 1998).

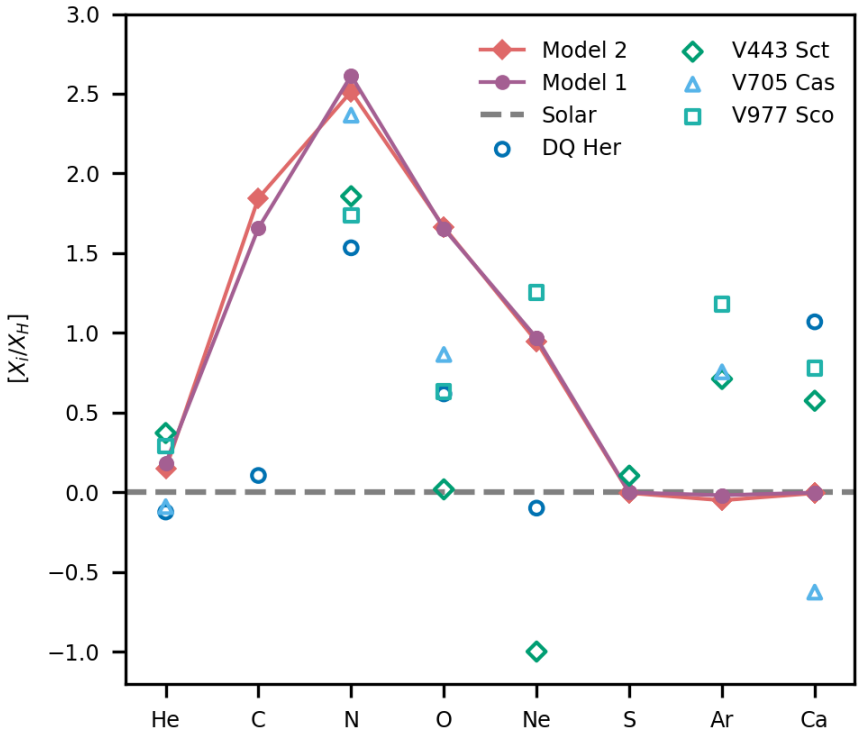

Figure 2.2: Comparison of observed abundances in CO novae V705 Cas (Arkhipova et al., 2000), V977 Sco (Andrea et al., 1994), V443 Sct (Andrea et al., 1994), and DQ Her (Pottasch, 1959) with predicted abundances from Model 1 and Model 2. Observational data are shown with blue and green symbols, while model predictions are represented by pink and purple circles and diamonds connected by a solid line.

In Fig. 2.2, the abundances of elements from He to Ca are plotted for Models 1 and 2 and compared against observations of novae that have been classified as the CO type. The mass fraction of H used to calculate $[X_i/X_H]$ is also taken from the mass averaged surface composition of the model nova envelope. For Model 1, this value is $X_H = 0.26$, for Model 2, this value is $X_H = 0.27$, with the initial value of H in the 50% pre-mixed accreted envelope being 0.35.

To accurately represent nucleosynthesis in our nova models, we must account for H depletion. Our results are presented as $[X_i/X_H]$, which can inaccurately represent X_i. This is because H gets depleted through H burning, meaning that $[X_i/X_H]$ can appear larger because the denominator has decreased. To address this, we subtract the logarithm of the ratio of H in the pre-mixed material to H in the envelope at the end of the simulations from our results. This adjustment quantifies H depletion and more accurately reflects the elements synthesized

during the explosion. In Figures 2.2 and 2.3, the model data have been downshifted by this factor to highlight changes resulting from nucleosynthesis. For a detailed explanation of this procedure, see Figure A.1 in the appendix.

As shown in Fig. 2.2, no Ca is produced in these models, which is expected for CO novae. However, the abundances of Ca from observations of CO novae exceed by nearly one order of magnitude both the solar and our predicted Ca abundances. Considering that CO novae reach lower peak TNR temperatures the presence of considerable overabundances of heavy elements in CO novae is unexpected. Furthermore, Ar also appears to be overabundant in these CO novae, which will be discussed in more detail in Section 3.1.

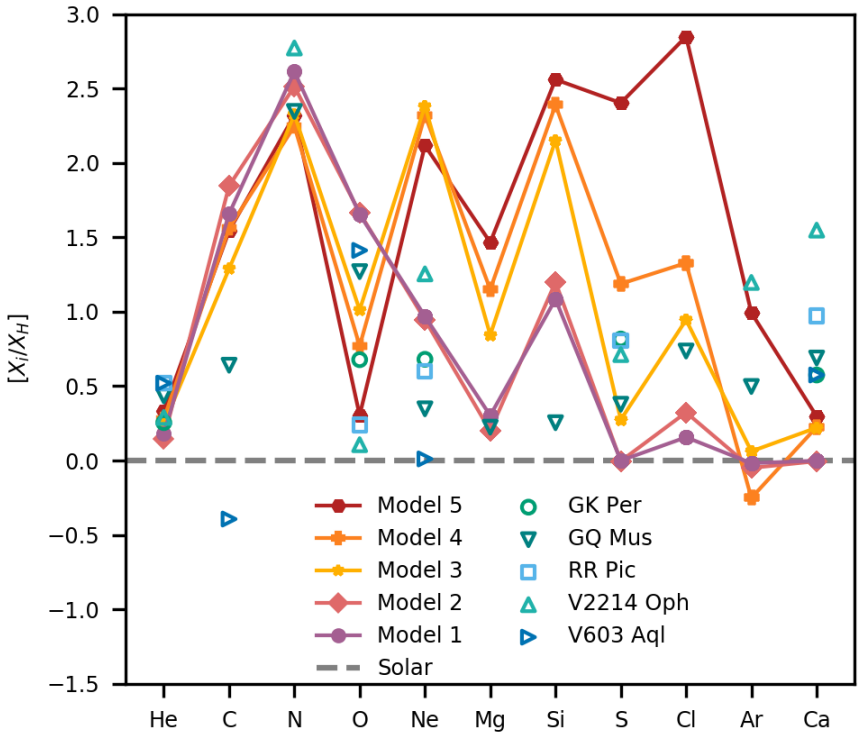

Figure 2.3: Comparison of observed abundances in novae of uncertain type (CO or ONe) with predicted abundances from multi-zone nova models. Observational data for V1224 Oph (Andrea et al., 1994), GQ Mus (Morisset & Pequignot, 1996), V603 Aql (Pottasch, 1959), RR Pic (Pottasch, 1959), and GK Per (Pottasch, 1959) are shown with blue and green symbols. Model predictions are represented by purple, pink, yellow, orange, and red symbols connected by solid lines.

In Fig. 2.3, all of our multi-zone nova models are compared with observations. In these observations, novae were not explicitly classified as either CO- or ONe-type novae. For the

ONe nova models in this figure, the mass fraction of hydrogen used to calculate $[X_i/X_H]$ was 0.26 for Model 3, 0.23 for Model 4, and 0.16 for Model 5. The observations of Ca seem to be overabundant compared to all models, including our hottest nova model that produces the largest amount of Ca. Due to the very low accretion rate of Model 5 and, as a result, a long period between its subsequent explosions, it is statistically highly unlikely that such a nova would be observed. Therefore, it is surprising that the observations show Ca abundances that are much higher than in our hottest nova model for a relatively large number of novae. This discrepancy may indicate that there is a significant error associated with the observations of Ca, and probably other heavy-element abundances around it. If the error of these measurements is indeed large, then there could be agreement between the observations and model predictions within those large error bars. However, for the observations used in our analysis, the declared uncertainties in abundances range from 20–30% (Evans et al., 2003; Arkhipova et al., 2000) to a factor of 2 or 3 (Andrea et al., 1994), and cannot account for the discrepancy between the observed and predicted Ca abundances.

2.4 Impact of Nuclear Physics Uncertainties

2.4.1 Single-zone Monte Carlo Simulations

One of the possible sources of uncertainties in our nova models is associated with the nuclear physics inputs, namely with the charged-particle reaction rates. To investigate the impact on Ca production, we initially focused on reaction rates in a "box" around Ca, varying them randomly within their estimated uncertainty ranges. This targeted approach was motivated by our aim to identify potential local nuclear physics solutions that could explain the observed Ca overabundance without significantly altering the abundances of other elements, which our models already match reasonably well for many novae. We performed a series of Monte Carlo (MC) simulations for each of our five one-zone nova models, as well as for our hottest multi-zone nova model. Specifically, we vary the reaction rates for isotopes ranging from ^{33}Cl to ^{41}Cl and up to isotopes from ^{38}Ti to ^{46}Ti. We include four types of charged-particle reactions in our MC simulations, namely (p,γ), (p,α), (α,p), and (α,γ). Only reactions for isotopes in a box around Ca are selected for this investigation because of our interest in reactions that may impact the Ca production locally, rather than globally. Otherwise, if we also, for example, increased rates of some reactions in the CNO cycle, we would certainly see, which we actually did, an increase in the production of Ca, along with other heavy elements. That would be caused by the possibility that a larger portion of the initially strongly enhanced mass fractions of C and O, or O and Ne, in the 50% pre-mixed envelopes of CO and ONe nova

models, respectively, would be carried by reaction fluxes towards the Ca region. However, the observations only seem to point out the overabundances of Ca and Ar in novae, as opposed to heavy elements in general. To provide a comprehensive analysis, we also conducted full-network MC simulations for our hottest multi-zone nova model, allowing us to compare results from both localized and full-network studies as discussed in Section 2.4.2.

For each one-zone nova model, we conduct 10,000 MC simulation runs, changing rates in the reaction network for each run. The method for doing these simulations is outlined in Denissenkov et al. (2021a). Two distinct sets of MC simulations are performed. In the first set, rates of all reactions in our selected box around Ca are randomly varied using a maximum variation factor of 10. Using a maximum variation factor of 10 for nuclear reaction rates reflects the uncertainties in reactions within this mass regime, particularly those with sparse nuclear level densities. The reaction rates are multiplied by factors spanning from 0.1 to 10 times the default reaction rate. This range is appropriate because of the potential influence of an unknown, strong, and narrow resonance that can significantly alter the reaction rate. For reactions with extensive experimental measurements or well-constrained resonance parameters, the uncertainty is often closer to a factor of 2 to 5. However, for reactions with minimal experimental data, the factor of 10 serves as a reasonable upper limit. This approach ensures that potential variations, particularly in reactions dominated by poorly understood resonances, are accounted for adequately. See Iliadis et al. (2002, 2010) for a more detailed discussion of reaction rate uncertainties.

Specifically, the rates of the four types of charged-particle reactions for 146 isotopes from Cl to Ti are randomly varied in ranges between the factor 10 down and up relative to their NuGrid default values[2], most of which are taken from the JINA Reaclib[3]. Given the sparse nuclear level densities in this atomic mass region, we choose this large rate uncertainty factor. To validate our findings, we perform a second set of MC simulations using maximum rate variation factors from the STARLIB database (Sallaska et al., 2013). The STARLIB database provides recommended reaction rates and their associated uncertainties across a range of temperatures, drawing from both theoretical and experimental sources. While verification ensures correct implementation of simulations and algorithms, validation assesses whether model predictions align with real-world behavior. The adoption of STARLIB variation factors supports this validation approach, as the library incorporates updated uncertainty factors based on experimental and theoretical data. Between the two sets of MC simulations, there

[2]The NuGrid default reaction rates for $^{37}\mathrm{K}(p,\gamma)^{38}\mathrm{Ca}$ and $^{38}\mathrm{K}(p,\gamma)^{39}\mathrm{Ca}$ were replaced with rates from the STARLIB library (Sallaska et al., 2013) and tested on our hottest nova model. There was a negligible change in the predicted composition.

[3]https://reaclib.jinaweb.org

are no qualitative differences in the results.

The main outcomes of these MC simulations are datasets comprising 10,000 distinct mass fraction sets for each element and isotope participating in nova nucleosynthesis. These datasets are analyzed to identify reactions whose rate uncertainties have the strongest impact on the predicted abundances of selected elements or isotopes. In this analysis, we calculate the Pearson product-moment correlation coefficients, $r_{\rm P}$, that quantify the strength of the link between the changes in reaction rates and variations of abundances they produce in the box around Ca, similar to how it was performed in Denissenkov et al. (2021a).

Table 2.2: Correlations and sensitivities revealed in one-zone Monte Carlo simulations with a maximum rate variation factor of 10. For each element, up to two reactions are shown if their Pearson correlation coefficients satisfy $|r_{\mathrm{P}}(f_i, X_k/X_{k,0})| \geq 0.15$. The last column displays the sensitivity factor ζ.

Nova Model	Element	Reaction	r_{P}[1]	ζ[2]
1	Ca	^{39}K(p,γ)	0.9757	0.0003416
	Ar	^{36}Ar(p,γ)	-0.9488	-0.1198
2	Ca	^{39}K(p,γ)	0.9022	0.001310
		^{38}Ar(p,γ)	0.2790	0.00040846
	Ar	^{36}Ar(p,γ)	-0.8192	-0.1644
		^{37}Ar(p,γ)	0.1682	0.03386
3	Ca	^{39}K(p,γ)	0.8061	0.008332
		^{38}Ar(p,γ)	0.3641	0.003794
	Ar	^{37}Ar(p,γ)	0.6815	0.2037
		^{36}Ar(p,γ)	-0.3752	-0.1118
4	Ca	^{39}K(p,γ)	0.3558	0.2340
		^{37}Ar(p,γ)	0.3059	0.2023
	Ar	^{35}Cl(p,γ)	0.5845	0.2699
		^{37}Ar(p,γ)	0.4109	0.1908
5	Ca	^{39}K(p,γ)	0.4132	0.4779
		^{38}K(p,γ)	0.3515	0.4083
	Ar	^{37}Ar(p,γ)	0.5359	0.1685
		^{35}Cl(p,γ)	0.4620	0.1444

Table 2.2 reveals which of the reaction rate variations, f_i has the strongest impact on the predicted abundance X_k, relative to their default value, $X_{k,0}$. The last two columns contained in this table are the corresponding Pearson correlation coefficients, r_{P}, and the parameter

[1] r_{P} is the Pearson coefficient estimating the correlation between the reaction rate variation and predicted abundance.

[2] ζ is a measure of the sensitivity of a given element to its correlated reaction.

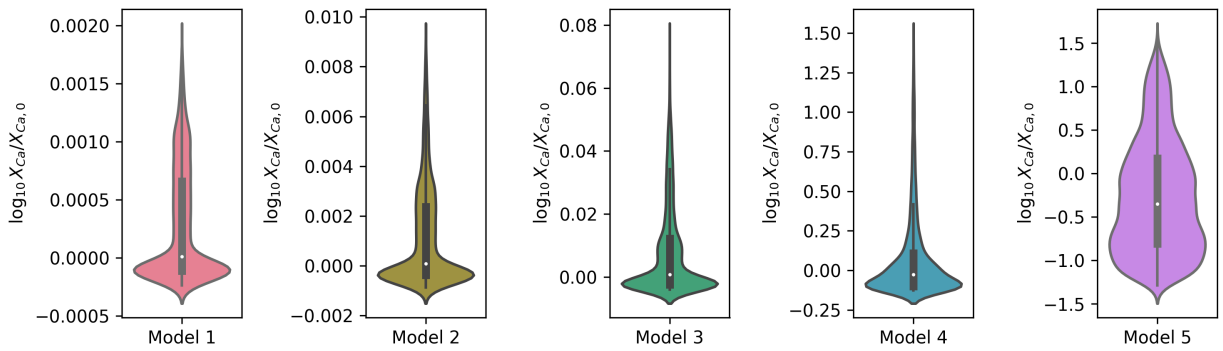

Figure 2.4: Distribution of Ca abundances from one-zone MC simulations relative to their benchmark values obtained using default NuGrid reaction rates for each model. Note the varying y-axis scale across panels.

ζ, which measures the sensitivity of that reaction in producing the desired element. This sensitivity parameter is calculated to be the slope of the line of best fit when we examine the reaction rate variation factors and the resulting elemental abundances as compared to their default values.

It is evident from the single-zone MC simulations that $^{39}\mathrm{K}(p,\gamma)^{40}\mathrm{Ca}$ has the strongest impact on the predicted Ca abundance, as one would expect given that this is a direct channel for producing the main stable isotope of Ca. As the peak temperature of the nova explosion increases among the models, the strength of the correlation between Ca and $^{39}\mathrm{K}(p,\gamma)^{40}\mathrm{Ca}$ decreases, and other reactions, namely $^{38}\mathrm{K}(p,\gamma)^{39}\mathrm{Ca}$ and $^{37}\mathrm{Ar}(p,\gamma)^{38}\mathrm{Ca}$, begin to contribute more strongly to the production of Ca.

The strength of the correlation is indicated by a value of the Pearson correlation coefficient, $\mathrm{r_P}$. Model 1, for example, exhibits a strong correlation but a narrow range of predicted Ca abundances, reflecting a weak sensitivity. In contrast, Model 5 shows a weaker correlation but a wider spread of calculated Ca abundances, as illustrated in Fig. 2.4. A weak sensitivity, as seen for Model 1, suggests that any increase in the $^{39}\mathrm{K}(p,\gamma)^{40}\mathrm{Ca}$ reaction rate would have a small effect on the abundance of Ca, as opposed to a strong sensitivity, as seen for Model 5, suggesting that a small variation in the reaction rate of $^{39}\mathrm{K}(p,\gamma)^{40}\mathrm{Ca}$ could change the abundance of Ca greatly.

2.4.2 Multi-zone Monte Carlo Simulation For The Hottest Nova Model

For the first time, we performed a reaction rate uncertainty study on a multi-zone nova model by running Monte Carlo post-processing nucleosynthesis simulations using the `MPPNP` code (Denissenkov et al., 2014, 2021a). `MPPNP` simulations account for time-dependent mixing

through detailed radial profiles of the temperature, density, and diffusion coefficient, while the single-zone simulations only use a temperature and density trajectory and do not consider mixing. One-zone simulations are faster and less computationally expensive and can be used for impact studies to estimate the importance of nuclear physics uncertainties. However, for a more confident analysis of nucleosynthesis in stars, we need to include all the physics relevant to this process, which is why multi-zone simulations are preferred for both individual and MC simulation runs and for comparison with observations.

We calculate two sets of multi-zone MC simulations. The first set uses the same method as its single-zone counterpart; only reactions in a box around Ca are varied by a factor of 10 up and down. The second set varies (p,γ), (p,α), (α,p), and (α,γ) reactions from H to Ti and uses the reaction rate variation factors from the STARLIB library (Sallaska et al., 2013). `MPPNP` is run using 1000 different simulations, each with a unique reaction network featuring randomly varied rates for selected reactions. On eight core processing units, each `SPPN` calculation takes a few minutes to run, whereas one `MPPNP` nova simulation usually takes a few hours. For this reason, we compute 1000 `MPPNP` simulations instead of the 10,000 used for single-zone calculations. We demonstrate in this paper that while single-zone MC simulations are sufficient to establish key correlations, multi-zone simulations provide the most accurate results. Our approach with 1000 multi-zone simulations balances accuracy and computational efficiency. We chose our hottest nova model for these simulations as it produces the most Ca compared to other models.

Figure 2.5 illustrates the distribution of Ca abundances relative to the default value for both sets of multi-zone MC simulations. The color intensity and size of the circles indicate the frequency of abundance occurrences, similar to Figure 2.4, but for multiple elements. Notably, the range of possible Ca abundances decreases from approximately three orders of magnitude in one-zone MC simulations to about one order of magnitude in multi-zone MC simulations. The bottom panel demonstrates that lighter elements generally exhibit less abundance variation, consistent with well-measured reaction rates for these elements. Conversely, elements near Ca show a larger abundance distribution, reflecting the greater uncertainties in charged-particle reaction rates in this mass region. While a limited reaction network is suitable for rapidly identifying key reactions, the detailed network more accurately represents nova environments. The observed decrease in abundance spread when expanding from a limited to a fuller reaction network in the MC simulations can be attributed to different maximum reaction rate variation factors: a factor of 10 for the limited network versus STARLIB library factors for the full network (Sallaska et al., 2013).

Table 2.3: Correlations and sensitivities revealed in our multi-zone MC simulation for Model 5 varying isotopes from Cl to Ti, with maximum reaction rate variation factors of 10 up and down. Two correlations are shown for each element if $|r_{\rm P}(f_i, X_k/X_{k,0})| \geq 0.15$.

Element	Reaction	$r_{\rm P}$	ζ
Cl	^{35}Cl(p,γ)	-0.4421	-0.03132
	^{36}Ar(p,γ)	0.4411	0.03140
Ar	^{35}Cl(p,γ)	0.6364	0.3100
	^{36}Ar(p,γ)	-0.4365	-0.2137
K	^{37}Ar(p,γ)	0.4733	0.2916
	^{38}K(p,γ)	0.4570	0.2807
Ca	^{39}K(p,γ)	0.5561	0.05681
	^{37}Ar(p,γ)	0.3147	0.03279

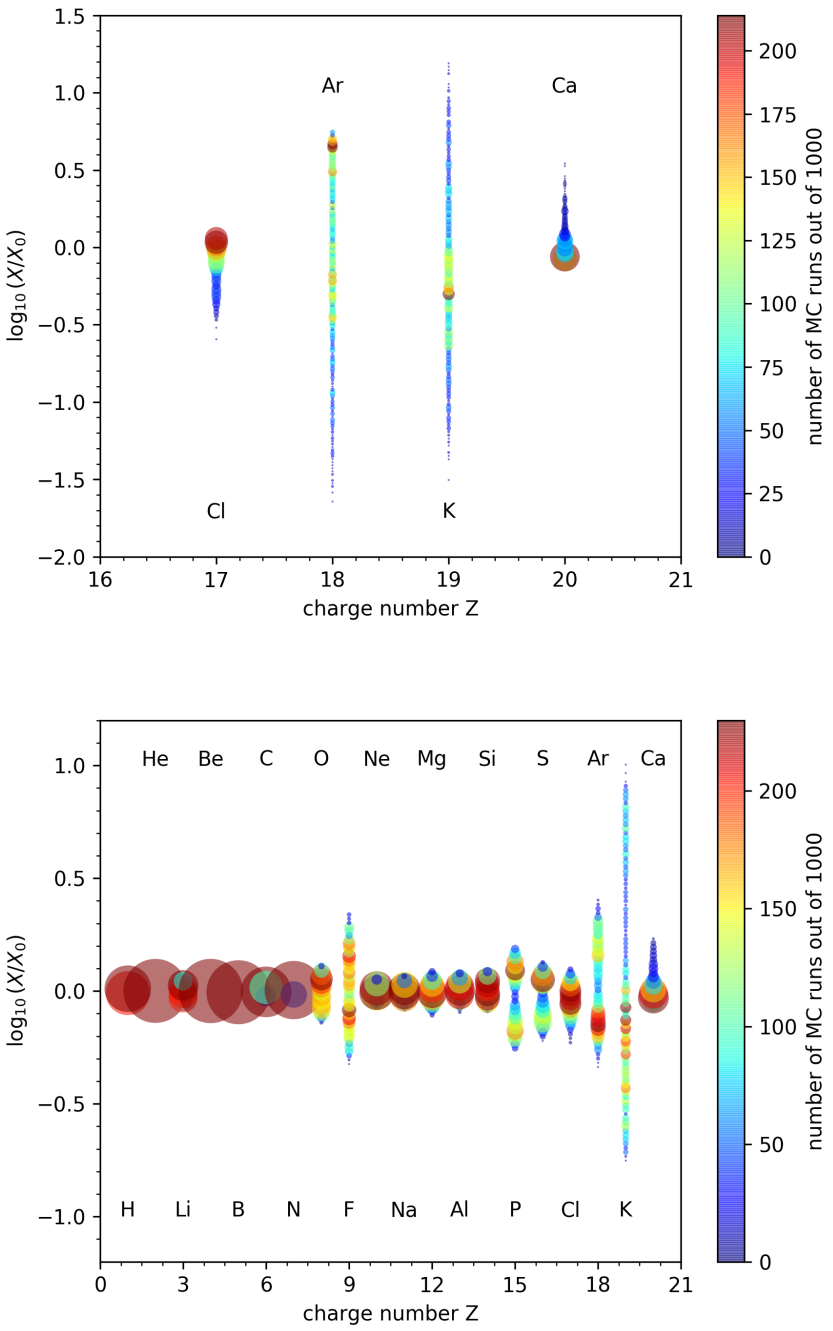

Figure 2.5: Distributions of the abundances for the selected elements relative to their default value in the multi-zone MC simulation for nova Model 5. The size and color of the circles represent the number of MC runs with that abundance. (Top panel: Limited network with maximum reaction rate variation factors of 10. Bottom panel: Full network, with maximum reaction rate variation factors from the STARLIB library (Sallaska et al., 2013).)

Table 2.4: Correlations and sensitivities revealed in the multi-zone Monte Carlo simulation for our hottest nova model. Reaction rates for isotopes from H to Ti were varied with maximum reaction rate variation factors from the STARLIB library (Sallaska et al., 2013). Two correlations are shown for each element if $|r_{\rm P}(f_i, X_k/X_{k,0})| \geq 0.15$.

Element	Reaction	$r_{\rm P}$	ζ
O	^{17}F(p,γ)	-0.8150	-0.7237
F	^{18}F(p,γ)	0.8772	0.8333
	^{18}F(p,α)	-0.3186	-1.076
Ne	^{23}Mg(p,γ)	-0.2992	-0.1330
	^{23}Na(p,γ)	-0.2671	-0.2954
Na	^{23}Mg(p,γ)	-0.3109	-0.1433
	^{23}Na(p,γ)	-0.2611	-0.2820
Mg	^{23}Na(p,γ)	0.3839	0.4904
	^{26}Al^m(p,γ)[1]	-0.2732	-0.01114
Al	^{23}Na(p,γ)	0.3221	0.3935
	^{25}Al(p,γ)	-0.2263	-0.0682
Si	^{30}P(p,γ)	-0.5124	-0.02173
	^{23}Mg(p,γ)	0.2207	0.1193
P	^{30}P(p,γ)	0.8154	0.07768
	^{31}P(p,γ)	-0.2024	-1.023
S	^{30}P(p,γ)	0.7407	0.04905
Cl	^{37}Ar(p,γ)	-0.4615	-0.02311
	^{30}P(p,γ)	0.3636	0.01769
Ar	^{37}Ar(p,γ)	0.8863	0.1399
K	^{37}Ar(p,γ)	0.6219	0.3928
	^{38}K(p,γ)	0.6005	0.3729
Ca	^{37}Ar(p,γ)	0.4496	0.02627
	^{38}K(p,γ)	0.4316	0.02479
	^{39}K(p,γ)	0.3419	0.1163

[1]This is the isomeric state of ^{26}Al.

2.4.3 Sensitivity of Important Reactions

Based on the key reactions identified in both single and multi-zone Monte Carlo simulations, we investigated their impact on calcium production. Our single-zone MC simulations indicated that increasing the rate of the ^{39}K$(p,\gamma)^{40}$Ca reaction could potentially enhance Ca abundance in multi-zone nova simulations. Longland et al. (2018) conducted an in-depth study of this reaction, revealing greater uncertainty in its rate than previously thought, particularly within the temperature range relevant to nova nucleosynthesis. More recently, Fox et al. (2024) proposed that the ^{39}K$(p,\gamma)^{40}$Ca reaction rate should be increased by a factor of 13 at 7×10^7 K. In light of these findings, we recomputed our hottest multi-zone nova model, increasing only the ^{39}K$(p,\gamma)^{40}$Ca reaction rate by a factor of 10 in our nuclear reaction network. This new simulation showed only a minimal increase in Ca production, insufficient to match the observed Ca abundances. The nuclear physics uncertainties could be a factor of 100, for example, if there is a narrow hidden resonance. For completeness, we also tested this case and found the increase was still minimal. We also tested the ^{38}K$(p,\gamma)^{39}$Ca reaction, the second most correlated to Ca production, by increasing its rate by factors of 10 and 100. More importantly, there is a depletion of Ar in both of these scenarios. This is an issue since the observations seem to suggest an overabundance of both Ca and Ar.

Table 2.3 shows the most important reactions associated with the production of a given element for set one of the multi-zone MC simulations. Compared to its one-zone counterpart, the strength of the correlation between ^{39}K$(p,\gamma)^{40}$Ca and Ca has increased in the multi-zone case. Additionally, the second most important reaction is no longer ^{38}K$(p,\gamma)^{39}$Ca but instead ^{37}Ar$(p,\gamma)^{38}$K.

Table 2.4 shows the most important reactions associated with the production of a given element for set two of the multi-zone MC simulations. We see that for Ar, K, and Ca, they all share the same important reactions, namely ^{37}Ar(p,γ) and ^{38}K(p,γ). In performing all of these MC simulations, we gain more realistic models that are needed to explore these abundance discrepancies. Specifically, going from the single-zone MC simulations to the multi-zone was necessary because, as previously discussed, `MPPNP` is more physical as it takes into account mixing. The next step was to go from a small network of reactions to a larger network. In doing so, we account for any reactions before Cl that may impact the abundance of Ar and Ca.

After identifying the important reactions from the multi-zone MC simulations, we can then individually vary their reaction rates in the MPPNP simulations. We find that increasing the ^{37}Ar(p,γ) rate by a factor of 10 and 100 in Model 5 increases the abundance of Ar to

better match the observations. This change also slightly increases Ca abundance, but not sufficiently to reach the observed levels.

2.4.4 Hot CNO breakout via The $^{19}\mathbf{F}(\boldsymbol{p},\gamma)^{20}\mathbf{Ne}$ Reaction

Novae on WDs with low central temperatures and accretion rates have peak TNR temperatures high enough for breakout from the hot CNO cycle to occur (Glasner & Truran, 2009). This may happen through the $^{19}\mathrm{F}(p,\gamma)^{20}\mathrm{Ne}$ reaction. If this reaction proceeds faster than $^{19}\mathrm{F}(p,\alpha)^{16}\mathrm{O}$, which closes the cycle CNO-IV, there is a possibility for breakout, and thus for heavier elements to be made. Clarkson & Herwig (2021) showed that if the ratio of the NACRE reaction rates for $^{19}\mathrm{F}(p,\gamma)/^{19}\mathrm{F}(p,\alpha)$ were increased by a factor of roughly 10, that might be able to account for the observations of Ca production in extremely metal-poor stars that had been polluted by material from their massive Population-III counterparts. Table 2.1 shows that the peak temperature for Model 5 is around 400 MK, which is high enough for breakout to occur. In this paper, we conduct a similar investigation by increasing the branching ratio of $^{19}\mathrm{F}(p,\gamma)/^{19}\mathrm{F}(p,\alpha)$ by a factor of 10 in the post-processing nucleosynthesis simulation for our hottest multi-zone nova model. No noticeable impact on the Ca abundance is found from this change. As previously mentioned it is extreme, but could be possible to have a reaction rate in this mass region that is uncertain by a factor of 100. We also tested this for the branching ratio and, similarly to the factor of 10, no noticeable impact was observed. This is due to the fact that the envelopes of present-day novae are all much more metal-rich than Population-III stars, and the effect of the change of this reaction rate ratio is too weakly expressed. Therefore, any nuclear physics uncertainties in this branching ratio are unlikely to be an avenue for further heavy element enhancement in our nova models and are unable to account for the Ca discrepancy.

2.5 Impact of mixing

Representing the accreted material for novae with a mixture of 50% solar-composition material from the companion star and 50% material from the outer layers of the accreting WD is a widely accepted method. However, the exact mixing mechanisms are still uncertain, so an alternative mixing prescription may be more accurate for some novae.

Our observational sample is limited to novae with reported Ca abundances, which may represent a self-selected subset of novae, i.e. in order for the weak highly ionized Ca lines to be able to be observed in the first place, a high Ca abundance may have to be in place, and perhaps only an unusual subset of novae have such a high abundance. The C abundance

in some of these observations seems unusually low, especially for CO Novae. To investigate whether these peculiar elemental abundances could be explained by a different mixing scenario, we re-ran our MPPNP simulations with a modified mixing prescription. This consisted of 75% solar-composition material from the companion star and 25% material from the outer layers of the white dwarf, tested for both our hottest and coldest nova models (Models 1 and 5, respectively). By reducing the fraction of material mixed in from the accreting white dwarf to 25%, the overall C abundance decreases, as the solar-composition material from the companion star is relatively C-poor compared to the white dwarf. The results, shown in Fig. 2.6 indicate that neither scenario could reproduce the observed C abundances. Furthermore, the 25/75 mixing produces slightly less Ca than the 50/50 mixing, still an order of magnitude discrepant from observations. While it is beyond the scope of this work to speculate on the reasons behind the potential peculiarities of this sample, we note that the high Ca abundances necessary for detection may be accompanied by atypical abundances of other elements. Further observational investigation is needed.

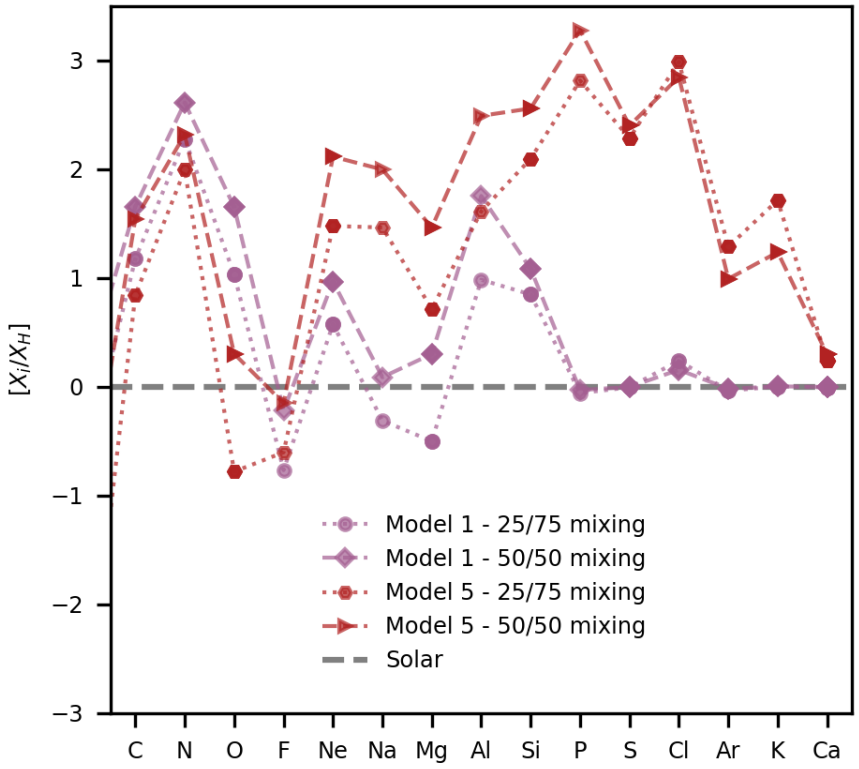

Figure 2.6: MPPNP abundances with different mixing prescriptions for Models 1 (in purple) and 5 (in red). The 50% solar-composition material and 50% WD material are denoted by dashed lines, and the 75% solar material and 25% WD material are denoted by dotted lines.

2.6 Results

In this paper, we have shown that there is a discrepancy between the observed and predicted abundances of Ca and Ar in novae, and have concluded that nuclear physics uncertainties cannot account for it, within the scope of the models used.

From the available literature, we gathered spectroscopic observations of novae containing Ca. Using the Nova Framework tools (Denissenkov et al., 2014), five nova models were made to represent the variety of novae that may be observed. In our comparative analysis between observed abundances and those predicted by our models, a notable discrepancy emerges. Specifically, Ca and Ar display consistent overabundances, up to one order of magnitude, in the observational data. Most striking is the difference between the observed CO novae and our CO nova model. No Ca is expected to be produced in these types of explosions because of their cooler peak TNR temperatures. Even the hottest nova model, Model 5,

is unable to reach the observed Ca and Ar abundances. However, because of the very low accretion rate for this model, the probability of observing such novae is low, suggesting that the observations we collected are unlikely to be from novae of this type.

This work focused on identifying and investigating the impact of nuclear physics uncertainties in our models and if these uncertainties are large enough to explain the difference in abundances. The rates at which the nuclear reactions take place in our network determine the final abundances. Some of these rates are not well measured experimentally, which leads to large uncertainties in their values. We performed several MC simulations on both single and multi-zone nova models with two distinct types of reaction variation. For the single-zone MC simulations, we performed two sets. The first varied reactions in a box around Ca by factors of 10 up and down and the second varied the same reactions but this time with variation factors from the STARLIB library (Sallaska et al., 2013). There were no qualitative differences found for the two sets of single-zone MC simulations. For the multi-zone MC simulations, we also performed two sets of calculations. The first varied reactions in a box around Ca by factors of 10 up and down, similar to the single-zone. The second set varied reactions from H to Ti by factors from the STARLIB library (Sallaska et al., 2013).

For the `SPPN` MC simulations for all 5 nova models, $^{39}\mathrm{K}(p,\gamma)^{40}\mathrm{Ca}$ was found to be the most strongly correlated to the production of Ca. When we increased its rate by a factor of 10 in the `MPPNP` simulation for our hottest nova model, the enhancement of the Ca abundance was minimal, nowhere close to any of the observations.

To confirm our findings from the one-zone nova MC simulations, we performed a multi-zone MC simulation for Model 5. This is the first time such simulations have been done in the context of nova nucleosynthesis. Using the multi-zone simulations to compare to observations or perform impact studies is crucial because they include more detailed physics than the one-zone simulations, such as mixing, which may play an important role in the nucleosynthesis. We found the spread in possible Ca abundances to decrease from $\sim 3\,\mathrm{dex}$ to $\sim 1\,\mathrm{dex}$ when going from the one-zone MC to multi-zone MC simulations.

Going from the `SPPN` to the first set of `MPPNP` MC simulations, the most influential reaction for Ca remained consistent, while for Ar it shifted from $^{37}\mathrm{Ar}(p,\gamma)$ to $^{35}\mathrm{Cl}(p,\gamma)$. To identify the important reaction mechanisms for both Ca and Ar, we initially varied several reactions around Ca, then broadened our search to include each element from H to Ti. We found that $^{37}\mathrm{Ar}(p,\gamma)$ emerged as the key reaction for both Ca and Ar in this expanded analysis. Subsequently, we increased the reaction rates for $^{37}\mathrm{Ar}(p,\gamma)$, $^{38}\mathrm{K}(p,\gamma)$, $^{39}\mathrm{K}(p,\gamma)$, and $^{19}\mathrm{F}(p,\gamma)$ individually by factors of 10 and 100 in our hottest nova model. However, none of these rate increases were sufficient to reproduce the abundances observed in the nova

ejecta.

In summary, uncertainties in nuclear reaction rates in proximity to the K-Ar-Ca region of the nuclear chart are unlikely to resolve the discrepancy between observed and predicted Ca abundances in nova ejecta. Further observational and theoretical investigations into the composition of the companion stars, observational effects, and the nova environment are warranted to answer this open question. That being said, experimental measurements of reactions in the region remain important, such as those related to Na or K production, and can help to constrain nova nucleosynthesis models further and relate to observations of pre-solar grains and the study of globular clusters, for instance. It is also important to consider that the observed high Ca abundances may be correlated with other atypical elemental abundances in the observed sites (i.e., low carbon), leading to the question of whether the observed objects are a self-selecting sample that is not representative of all novae. In concert with advances in modeling, future multi-wavelength observations of a broad sample of nova events will be key to unraveling the mysteries still surrounding these dramatic yet common stellar explosions.

Chapter 3

Discussion

It has now been established that the nuclear physics uncertainties in our nova models, namely the estimated uncertainties of the charged-particle reaction rates, would not be able to account for the discrepancy between observations and our model predictions of the Ca abundance. In this section, alternative explanations of the Ca discrepancy are discussed along with the limitations of this work.

3.1 Alternative hypotheses explaining high Ca abundance in novae

One possible explanation for the overabundance of Ca in observations is that the accreted material originates from an evolved stellar companion. For example, Williams et al. (2016) found that approximately 20–40% of novae observed in the Andromeda Galaxy have a red giant companion. In this scenario, the accreted nova envelope would be enhanced in heavy elements instead of having solar composition (Darnley et al., 2012). It is possible in the Nova Framework to change the initial conditions to reflect such an enriched envelope, which could be the focus of future work. For instance, the effect of increasing ^{4}He abundance in the accreted nova envelope has been previously investigated by Denissenkov et al. (2021b). The authors showed that increasing ^{4}He in agreement with observational data of Gehrz et al. (1998) in nova models could reduce the discrepancy between the observed and predicted abundances of ^{7}Be in novae. The amount and metallicity of the accreted material have important implications for nucleosynthesis in these explosions. As discussed in the introduction, more accreted material means more nuclear fuel, which leads to more extreme explosions. More metal-rich material can also lead to the formation of more heavy elements. However, metal-rich material has a larger opacity, which means more heat will be trapped (Starrfield et al., 1998). The more heat that is trapped will cause the temperature of this material to increase faster which leads to the explosion happening more quickly. Therefore more material

will be accreted if the material is metal-poor because the temperature will rise more slowly (Starrfield et al., 2000). The initial metal content of the accreted material plays a crucial role in determining the final abundances of heavy elements. However, it is unclear whether the initial metallicity or the total mass accreted has a greater impact on heavy element production. This presents an interesting avenue for future research. Specifically, it would be valuable to investigate whether there is an optimal level of metal enrichment that allows for an extreme nova explosion while still producing significant amounts of heavy elements. Future studies could explore the interplay between initial metallicity, accretion mass, and heavy element nucleosynthesis to better understand the conditions that lead to the observed abundances in nova ejecta.

Another possible explanation for the observed overabundance of Ca is that the Ca is getting trapped in dust grains. Dust formation happens in the expanding ejecta as things cool and condense. The presence of dust grains is evidenced by a dip in the optical light curve (Chomiuk et al., 2021). This is because the optical photosphere is obscured by the dust formation. The dips in the optical spectra are complemented by increases in the mid-infrared spectra. Crinklaw et al. (1994) showed that Ca in the interstellar medium (ISM) tends to be converted into dust due to its high condensation temperature compared to other lighter mass elements. If Ca were to become trapped in the dust, which remains after the nova explosion, and these explosions were to happen recurrently, over time it may be possible that Ca builds up around a star relative to other light elements and thus appears overabundant in observations of novae. However, this theory is inconsistent when considering Ar. With its chemical properties being markedly different from Ca, we would not expect to see an enhancement in Ar in the dust fractionation scenario, as it would be blown away with other gases. Therefore, the simultaneous observational overabundance of both Ca and Ar questions dust fractionation as a viable explanation.

The Ca abundance in nova nucleosynthesis could also be reframed as a seed problem. In this scenario, the initial abundances of heavier elements act as seeds for proton capture and subsequent reactions. In CO WDs, C and O act as primary seeds whereas for ONe WDs, the seed elements include O, Ne, Mg, and trace amounts of Si, Ar, and Ca. For Ca production specifically, Ar and K serve as direct seeds through proton capture reactions. To better understand this, investigations into AGB stellar evolution to determine the maximum metal enrichment possible in ONe WDs could be conducted. The models in this work could also test this by increasing initial Ca seed abundances by factors of two to ten and analyzing the resulting final Ca abundance.

3.2 Limitations of This Work

This research, while comprehensive, has several limitations to consider. First and foremost, the observational dataset used was limited, comprising only nine novae with reported Ca abundances, most of which were observed over 20 years ago. Moreover, spectroscopic technology and analysis techniques have significantly advanced in the past two decades, particularly with the implementation of machine learning methods (Garcia-Dias et al., 2018). Additionally, the studies provided limited information on the uncertainties associated with their abundance measurements, which constrains our ability to make comparisons with the simulations. Specifically, if the error bars on the observed Ca abundances are sufficiently large, some measurements might be in agreement with the model predictions.

Another limitation is that, for time constraints, only 1,000 `MPPNP` MC simulations were performed as opposed to 10,000 for the `SPPN` simulations. In a direct MC simulation, the error goes as $\sigma/\sqrt{n}$ where n is the number of independent samples or the number of MC runs (Sharma, 2017). Therefore, increasing the number of runs from 1,000 to 10,000 reduces the error by approximately 31.6%. In this work, 1,000 runs are enough to see the key reactions with strong impacts; however, with more MC runs, reactions with a more moderate impact would also be seen. With fewer MC runs, there is a higher risk of false negatives, i.e., not identifying important reactions, or false positives i.e., incorrectly identifying unimportant ones as significant. Similarly, a large number of samples reduces the random sampling error meaning the correlation coefficients are less likely to fluctuate due to random chance. To test this, it would be beneficial to perform a convergence test to see what number of MC runs is needed for the correlation coefficients to not fluctuate, which could be the focus of future work.

Our multi-zone nova models identified $^{37}\mathrm{Ar}(p,\gamma)$ as the reaction most strongly correlated with the production of Ca. ^{37}Ar has a half-life of 35 days, decaying via electron capture. However, in the highly ionized plasma environment of novae, the decay rate of ^{37}Ar may be significantly altered. The extreme temperatures in novae can lead to nearly complete ionization of atoms, potentially reducing the availability of orbital electrons for capture. This effect could substantially extend the half-life of ^{37}Ar. It would be valuable to investigate the impact of treating ^{37}Ar as effectively stable on the Ca abundance in our nova models. However, $^{37}\mathrm{Ar}(p,\gamma)$ is not the only reaction responsible for Ca production; it works in tandem with the $^{38}\mathrm{K}(p,\gamma)$ and $^{39}\mathrm{K}(p,\gamma)$ reactions. It is possible that all three of these reactions may be uncertain and need to be increased at the same time. Accurate measurements of these reaction rates and their associated uncertainties would provide crucial constraints for the

simulations.

These limitations highlight the need for continued observational efforts, improved experimental measurements of key nuclear reactions, and further refinement of theoretical models to fully unravel the puzzle of Ca abundances in novae.

Chapter 4

Conclusions and Next Steps

4.1 Conclusion

This research found that observed levels of Ca and Ar in novae are higher than model predictions and solar abundances, and that nuclear physics uncertainties cannot account for this discrepancy. The impact of nuclear physics uncertainties on predicted abundances was investigated with MC simulations conducted on single-zone nova models, and, for the first time, this approach was applied to multi-zone nova models. From the MC simulations, $^{37}\mathrm{Ar}(p,\gamma)$, $^{38}\mathrm{K}(p,\gamma)$, and $^{39}\mathrm{K}(p,\gamma)$ were identified as the key reactions for the production of Ca. When these reactions were each increased by factors of 10 and 100, the Ca abundance did increase slightly, but not enough to reach the observations. The $^{19}\mathrm{F}(p,\gamma)/^{19}\mathrm{F}(p,\alpha)$ branching ratio was also increased by factors of 10 and 100 to test the impact of hot CNO cycle breakout; however, no change in the abundances was noted. Various mixing prescriptions were tested to explain the peculiar C abundance observed in some novae with high Ca levels, but these alternative mixing scenarios did not account for the observed abundance patterns. Ultimately, this work demonstrated that nuclear physics uncertainties cannot account for the Ca overabundance, and more work is needed to resolve this discrepancy.

4.2 Future Work

The work presented in this thesis has the potential to inspire future work in experimental nuclear physics, computational astrophysics, and observational astronomy.

As highlighted in Chapter 3, one of the main limitations of this work is the small sample size of the observations. This work motivates more targeted observations of novae, specifically focused on measuring Ca abundances. Furthermore, additional abundance estimates are necessary to determine whether a subset of novae exists with elevated Ca levels and atypical

abundances of other elements, such as C.

The nova models used in this work could be further applied to the study of pre-solar grains originating in novae, the impact of accretion from evolved companion stars, and the validation of nuclear physics uncertainties from experimental work. For example, Iliadis et al. (2018) identified 18 pre-solar grains that have measured isotopic signatures that match a CO nova origin, without assuming any dilution of the ejecta. Collaboration with Dr. Nan Liu has been proposed to further explore this avenue of research. Additionally, an investigation into the initial abundance of the simulations to mimic accretion from an evolved companion star is needed to investigate the impact of metallicity on accreted mass, heavy element synthesis, and peak TNR temperature. Finally, collaboration with Dr. Michael Wiescher has also been proposed as new reaction rates have been measured by his team for the reactions $^{39}\mathrm{K}(p,\gamma)$ and $^{40}\mathrm{Ca}(p,\gamma)$. These new rates will be incorporated into our most extreme model to examine the impact on the Ca abundance and to determine if material is driven into the Mn-Fe region.

Motivation for future nuclear physics experiments, particularly those focused on refining reaction rates directly, stems from the results of this research. To measure low-energy nuclear reactions relevant to astrophysical environments like novae, the DRAGON facility at TRIUMF can be used. Lotay & Ruiz (2023) have submitted a proposal for the measurement of the $^{37}\mathrm{Ar}(p,\gamma)$ reaction at DRAGON, which will take place in the near future. Since this reaction is key to the production of Ca in novae, a better-constrained rate would provide valuable input for the simulations. Given that ^{37}Ar is radioactive, using it as a radioactive ion beam is challenging. Without direct measurements, this reaction rate could vary by factors of 10, 100, or even more, underscoring the need for further investigation of this poorly studied reaction.

The work presented in this thesis can be used to test the results of my PhD work, involving the measurement of the $^{7}\mathrm{Be}(p,\gamma)^{8}\mathrm{B}$ reaction cross section in inverse kinematics using the DRAGON facility at TRIUMF. This measurement will address existing discrepancies in the forward kinematics data and provide essential input for solar neutrino flux calculations and nova nucleosynthesis models. Following the data analysis, the results will be incorporated into the nova models from this research. This work will build upon my MSc research using the Nova Framework, allowing for direct quantification of the new measurements' impact on astrophysical predictions.

The Ca abundance discrepancy in novae represents a significant challenge to both the current understanding of the nova environment and observational astronomy. The resolution of this discrepancy requires interdisciplinary collaboration between nuclear physics, astrophysics, and observational astronomy. For the nuclear physics community, this problem

highlights the need for more precise measurements of key reaction rates and underscores the importance of nuclear data in astrophysical modeling. While current nuclear physics uncertainties cannot fully explain the observed overabundance, this work guides future experimental efforts. Ultimately, resolving this discrepancy could have far-reaching implications for our understanding of element production in novae.

Bibliography

Ackermann, M., Ajello, M., Albert, A., et al. 2014, Science, 345, 554, doi: 10.1126/science.1253947

Ali, S. M., Santra, R., Sharma, S., & Mondal, A. K. 2024, , 109, 045809, doi: 10.1103/PhysRevC.109.045809

Amari, S., Gao, X., Nittler, L. R., et al. 2001, , 551, 1065, doi: 10.1086/320235

Andrea, J., Drechsel, H., & Starrfield, S. 1994, , 291, 869

Arkhipova, V. P., Burlak, M. A., & Esipov, V. F. 2000, Astronomy Letters, 26, 372, doi: 10.1134/1.20404

Bode, M. F., & Evans, A. 2008, Classical Novae, Vol. 43, doi: 10.1017/CBO9780511536168

Casanova, J., José, J., García-Berro, E., Calder, A., & Shore, S. N. 2010, , 513, L5, doi: 10.1051/0004-6361/201014178

Casanova, J., José, J., García-Berro, E., Shore, S. N., & Calder, A. C. 2011, , 478, 490, doi: 10.1038/nature10520

Chen, M. C., Herwig, F., Denissenkov, P. A., & Paxton, B. 2014, , 440, 1274, doi: 10.1093/mnras/stu108

Chomiuk, L., Metzger, B. D., & Shen, K. J. 2021, , 59, 391, doi: 10.1146/annurev-astro-112420-114502

Chugai, N. N., & Kudryashov, A. D. 2020, arXiv e-prints, arXiv:2007.07044, doi: 10.48550/arXiv.2007.07044

Clarkson, O., & Herwig, F. 2021, , 500, 2685, doi: 10.1093/mnras/staa3328

Crinklaw, G., Federman, S. R., & Joseph, C. L. 1994, , 424, 748, doi: 10.1086/173927

Darnley, M. J., Ribeiro, V. A. R. M., Bode, M. F., Hounsell, R. A., & Williams, R. P. 2012, , 746, 61, doi: 10.1088/0004-637X/746/1/61

Darnley, M. J., Bode, M. F., Kerins, E., et al. 2006, Monthly Notices of the Royal Astronomical Society, 369, 257, doi: 10.1111/j.1365-2966.2006.10297.x

Denissenkov, P. A., Herwig, F., Bildsten, L., & Paxton, B. 2013, , 762, 8, doi: 10.1088/0004-637X/762/1/8

Denissenkov, P. A., Herwig, F., Perdikakis, G., & Schatz, H. 2021a, , 503, 3913, doi: 10.1093/mnras/stab772

Denissenkov, P. A., Ruiz, C., Upadhyayula, S., & Herwig, F. 2021b, , 501, L33, doi: 10.1093/mnrasl/slaa190

Denissenkov, P. A., Truran, J. W., Pignatari, M., et al. 2014, , 442, 2058, doi: 10.1093/mnras/stu1000

Doherty, C. L., Gil-Pons, P., Siess, L., Lattanzio, J. C., & Lau, H. H. B. 2015, , 446, 2599, doi: 10.1093/mnras/stu2180

Downen, L., Iliadis, C., Champagne, A., et al. 2022, , 928, 128, doi: 10.3847/1538-4357/ac582b

Duquennoy, A., & Mayor, M. 1991, , 248, 485

European Southern Observatory. 2007, Hertzsprung-Russell Diagram. https://www.eso.org/public/images/eso0728c/

Evans, A., Gehrz, R. D., Geballe, T. R., et al. 2003, , 126, 1981, doi: 10.1086/377618

Fox, W., Longland, R., Marshall, C., & Chaves, F. P. 2024, , 132, 062701, doi: 10.1103/PhysRevLett.132.062701

Fujimoto, M. Y., & Taam, R. E. 1982, , 260, 249, doi: 10.1086/160251

Garcia-Dias, R., Allende Prieto, C., Sánchez Almeida, J., & Ordovás-Pascual, I. 2018, , 612, A98, doi: 10.1051/0004-6361/201732134

Gehrz, R. D., Truran, J. W., Williams, R. E., & Starrfield, S. 1998, , 110, 3, doi: 10.1086/316107

Giannone, P., & Weigert, A. 1967, , 67, 41

Glasner, S. A., & Truran, J. W. 2009, , 692, L58, doi: 10.1088/0004-637X/692/1/L58

Glasner, S. A., & Truran, J. W. 2012, in Journal of Physics Conference Series, Vol. 337, Journal of Physics Conference Series (IOP), 012071, doi: 10.1088/1742-6596/337/1/012071

Grevesse, N., & Noels, A. 1993, Physica Scripta Volume T, 47, 133, doi: 10.1088/0031-8949/1993/T47/021

Herwig, F. 2005, , 43, 435, doi: 10.1146/annurev.astro.43.072103.150600

—. 2013, in Planets, Stars and Stellar Systems. Volume 4: Stellar Structure and Evolution, ed. T. D. Oswalt & M. A. Barstow, Vol. 4, 397, doi: 10.1007/978-94-007-5615-1_8

Herwig, F., Diehl, S., Fryer, C. L., et al. 2008, in Nuclei in the Cosmos (NIC X), E23, doi: 10.22323/1.053.0023

Hix, W. R., Smith, M. S., Starrfield, S., Mezzacappa, A., & Smith, D. L. 2003, , 718, 620, doi: 10.1016/S0375-9474(03)00904-7

Iliadis, C. 2015, Nuclear physics of stars, doi: 10.1002/9783527692668

Iliadis, C., Champagne, A., José, J., Starrfield, S., & Tupper, P. 2002, , 142, 105, doi: 10.1086/341400

Iliadis, C., Downen, L. N., José, J., Nittler, L. R., & Starrfield, S. 2018, , 855, 76, doi: 10.3847/1538-4357/aaabb6

Iliadis, C., Longland, R., Champagne, A. E., & Coc, A. 2010, , 841, 251, doi: 10.1016/j.nuclphysa.2010.04.010

Izzo, L., Della Valle, M., Mason, E., et al. 2015, , 808, L14, doi: 10.1088/2041-8205/808/1/L14

José, J., Coc, A., & Hernanz, M. 2001, , 560, 897, doi: 10.1086/322979

José, J., & Hernanz, M. 1998, , 494, 680, doi: 10.1086/305244

—. 2007a, Journal of Physics G Nuclear Physics, 34, R431, doi: 10.1088/0954-3899/34/12/R01

—. 2007b, , 42, 1135, doi: 10.1111/j.1945-5100.2007.tb00565.x

José, J., Shore, S. N., & Casanova, J. 2020, , 634, A5, doi: 10.1051/0004-6361/201936893

Kenyon, S. J., & Truran, J. W. 1983, , 273, 280, doi: 10.1086/161367

Kippenhahn, R., Weigert, A., & Weiss, A. 2013, Stellar Structure and Evolution, doi: 10.1007/978-3-642-30304-3

Longland, R., & de Séréville, N. 2020, , 642, A41, doi: 10.1051/0004-6361/202038151

Longland, R., Dermigny, J., & Marshall, C. 2018, , 98, 025802, doi: 10.1103/PhysRevC.98.025802

Lotay, G., & Ruiz, C. 2023

Mikolajewska, J. 2010, arXiv e-prints, arXiv:1011.5657, doi: 10.48550/arXiv.1011.5657

Morisset, C., & Pequignot, D. 1996, , 312, 135

Mumpower, M. R., Sprouse, T. M., Miller, J. M., et al. 2024, , 970, 173, doi: 10.3847/1538-4357/ad5afc

NASA/CXC/RIKEN/D.Takei et al., NASA/STScI, N. 2015, GK Persei - Classical Nova, https://chandra.harvard.edu/photo/2015/gkper/more.html

Paczynski, B., & Zytkow, A. N. 1978, , 222, 604, doi: 10.1086/156176

Paxton, B., Bildsten, L., Dotter, A., et al. 2011, , 192, 3, doi: 10.1088/0067-0049/192/1/3

Paxton, B., Cantiello, M., Arras, P., et al. 2013, , 208, 4, doi: 10.1088/0067-0049/208/1/4

Pignatari, M., Herwig, F., Hirschi, R., et al. 2016, , 225, 24, doi: 10.3847/0067-0049/225/2/24

Pottasch, S. 1959, Annales d'Astrophysique, 22, 412

Prialnik, D., & Kovetz, A. 1995, , 445, 789, doi: 10.1086/175741

Ruiz, C., Parikh, A., José, J., et al. 2006, , 96, 252501, doi: 10.1103/PhysRevLett.96.252501

Sallaska, A. L., Iliadis, C., Champange, A. E., et al. 2013, , 207, 18, doi: 10.1088/0067-0049/207/1/18

Sallaska, A. L., Wrede, C., García, A., et al. 2010, , 105, 209901, doi: 10.1103/PhysRevLett.105.209901

Shafter, A. W. 2017a, , 834, 196, doi: 10.3847/1538-4357/834/2/196

—. 2017b, , 834, 196, doi: 10.3847/1538-4357/834/2/196

Shapley, H. 1917, , 29, 213, doi: 10.1086/122669

Sharma, S. 2017, , 55, 213, doi: 10.1146/annurev-astro-082214-122339

Sion, E. M., Acierno, M. J., & Tomczyk, S. 1979, , 230, 832, doi: 10.1086/157143

Starrfield, S., Bose, M., Iliadis, C., et al. 2021, in The Golden Age of Cataclysmic Variables and Related Objects V, Vol. 2-7, 30, doi: 10.22323/1.368.0030

Starrfield, S., Iliadis, C., & Hix, W. R. 2016, , 128, 051001, doi: 10.1088/1538-3873/128/963/051001

Starrfield, S., Schwarz, G., Truran, J. W., & Sparks, W. M. 2000, in American Institute of Physics Conference Series, Vol. 522, Cosmic Explosions: Tenth AstroPhysics Conference, ed. S. S. Holt & W. W. Zhang (AIP), 379–382, doi: 10.1063/1.1291739

Starrfield, S., Truran, J. W., Wiescher, M. C., & Sparks, W. M. 1998, , 296, 502, doi: 10.1046/j.1365-8711.1998.01312.x

Starrfield, S. G., Watson, T. J., Sparks, W. M., Truran, J. W., & Kutter, G. S. 1971, in Bulletin of the American Astronomical Society, Vol. 3, 484

Warner, B. 1995, Cataclysmic variable stars, Vol. 28

Williams, M., Lennarz, A., Laird, A. M., et al. 2020, , 102, 035801, doi: 10.1103/PhysRevC.102.035801

Williams, S. C., Darnley, M. J., Bode, M. F., & Shafter, A. W. 2016, , 817, 143, doi: 10.3847/0004-637X/817/2/143

Woodward, C. E., Banerjee, D. P. K., Geballe, T. R., et al. 2021, , 922, L10, doi: 10.3847/2041-8213/ac3518

Appendix A

Additional Information

Figure A.1 illustrates the distinct impacts of initial mixing and nucleosynthesis on elemental abundances in our analysis. The blue line represents abundances in the pre-mixed material, while the red line shows abundances after the nova explosion. Abundances from the blue line that are above solar levels (dashed line) indicate elements in the pre-mixed material that were already enhanced prior to the nova event. In contrast, abundances from the red line that lie above the dotted line (representing the ratio of initial H to H in the envelope after the explosion) represent elements produced through nucleosynthesis during the nova event. By comparing the initial and final H abundances, we can quantify H depletion due to H burning, which serves as an indicator of the extent of nuclear processing. This representation is crucial because it prevents misinterpretation of the data. For instance, in Model 1, elements like Ar, K, and Ca might appear overabundant when the red line is compared directly to solar abundance. However, this apparent overabundance is primarily due to H depletion rather than significant nucleosynthesis of these elements. To accurately represent nucleosynthesis in our nova models, we must account for this hydrogen depletion. Our results are presented as $[X_i/X_H]$, which can overestimate X_i if H decreases. To address this, we subtract the logarithm of the ratio of H in the pre-mixed material to H in the envelope at the end of the simulations from our results. This adjustment quantifies H depletion and more accurately reflects the elements synthesized during the explosion. Consequently, to accurately display which elements are synthesized in the explosion, all models in Figures 2.2 and 2.3 have been downshifted by this H-depletion factor. This approach allows us to clearly distinguish between abundance changes resulting from the use of pre-mixed material and those truly arising from nucleosynthesis during the nova event.

A detailed breakdown of the nova observations is provided in Table A.1. For each nova, the number density and corresponding mass fraction are reported. The methodology for converting from number density to mass fraction is described by equations 2.1–2.3.

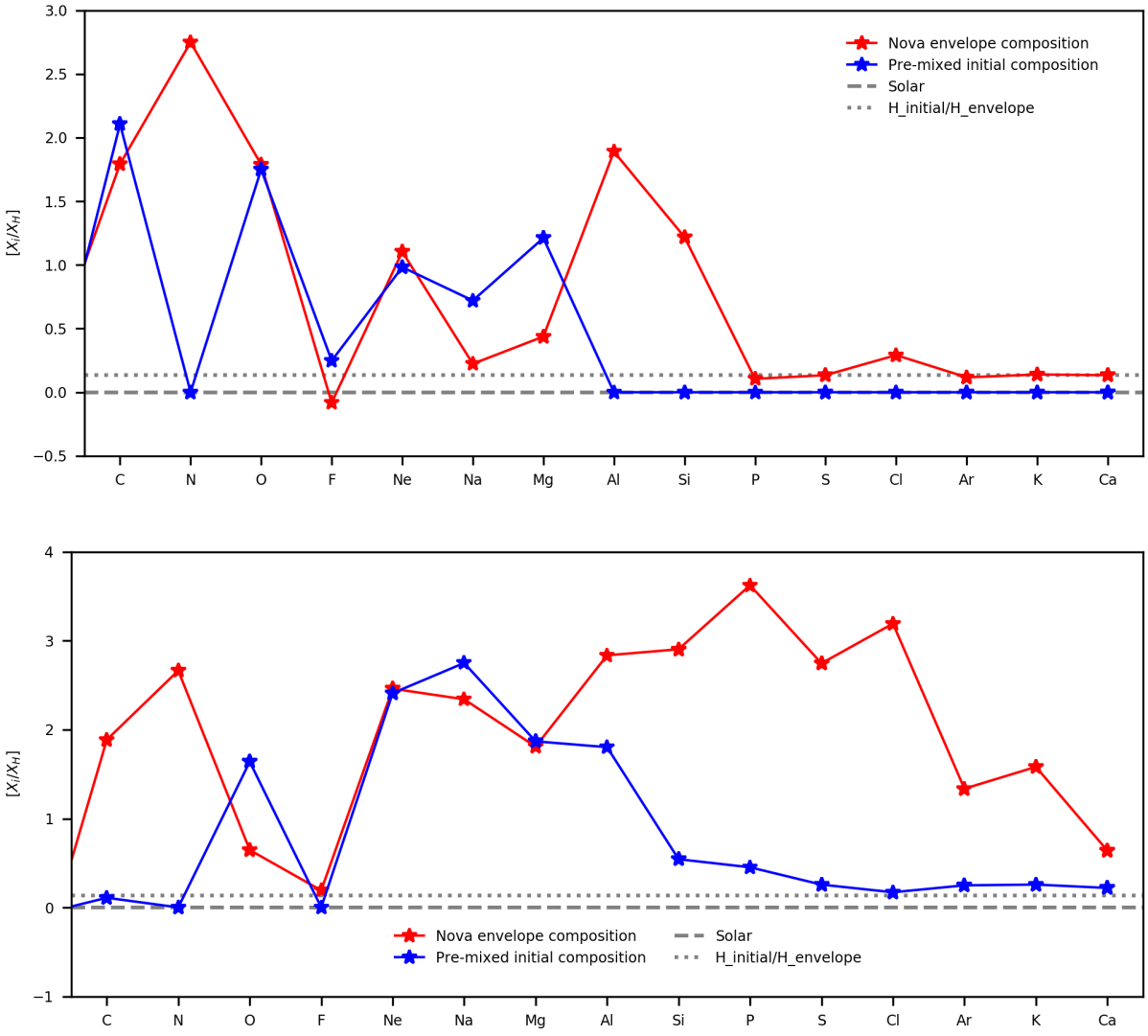

Figure A.1: Comparison of elemental mass fractions from the pre-mixed initial composition representing the accreted envelope (blue line) and the envelope composition (red line) in our multi-zone nova models. The dashed line shows the solar composition and the dotted line shows the difference in H between the initial composition and the envelope. The top panel shows this for Model 1 and the bottom panel shows this for Model 5. For both of the models shown the pre-mixed material is assumed to be 50% solar material and 50% WD material.

Table A.1: Observed Nova Abundances

Nova	(N_{He}/N_H)	(N_C/N_H)	(N_N/N_H)	(N_O/N_H)	(N_{Ne}/N_H)
			Pottasch (1959)		
V603 Aql	3.23E-1	1.67E-4	-	2.22E-2	1.43E-4
X_i/X_H	1.28E0	1.99E-3	-	3.53E-1	2.86E-3
DQ Her	7.35E-2	5.26E-4	3.70E-3	3.57E-3	1.11E-4
X_i/X_H	2.92E-1	6.27E-3	5.15E-2	5.67E-2	2.22E-3
GK Per	1.75E-1	-	-	4.10E-3	6.67E-4
X_i/X_H	6.97E-1	-	-	6.50E-2	1.33E-2
RR Pic	3.23E-1	-	-	1.49E-3	5.56E-4
X_i/X_H	1.28E0	-	-	2.37E-2	1.11E-2
			Andrea et al. (1994)		
V2214 Oph	1.90E-1	-	6.40E-2	1.10E-3	2.50E-3
X_i/X_H	7.54E-1	-	8.89E-1	1.75E-2	5.00E-2
V977 Sco	1.90E-1	-	5.90E-3	3.70E-3	2.50E-3
X_i/X_H	7.54E-1	-	8.20E-2	5.87E-2	5.00E-2
V443 Sct	2.30E-1	-	7.80E-3	9.00E-4	1.40E-5
X_i/X_H	9.13E-1	-	1.08E-1	1.43E-2	2.80E-4
			Morisset & Pequignot (1996)		
GQ Mus	2.65E-1	1.80E-3	2.40E-2	1.60E-2	3.10E-4
X_i/X_H	1.05E0	2.14E-2	3.34E-1	2.54E-1	6.21E-3
			Arkhipova et al. (2000)		
V705 Cas	7.94E-2	-	2.51E-2	6.31E-3	-
X_i/X_H	3.15E-1	-	3.49E-1	1.00E-1	-

Table A.1: Continued

Nova	(N_{Mg}/N_H)	(N_{Si}/N_H)	(N_S/N_H)	(N_{Cl}/N_H)	(N_{Ar}/N_H)	(N_{Ca}/N_H)
			Pottasch (1959)			
V603 Aql	-	-	-	-	-	1.00E-5
X_i/X_H	-	-	-	-	-	3.98E-4
DQ Her	-	-	-	-	-	3.13E-5
X_i/X_H	-	-	-	-	-	1.24E-3
GK Per	-	-	1.23E-4	-	-	1.00E-5
X_i/X_H	-	-	3.93E-3	-	-	3.98E-4
RR Pic	-	-	1.20E-4	-	-	2.50E-5
X_i/X_H	-	-	3.83E-3	-	-	9.94E-4
			Andrea et al. (1994)			
V2214 Oph	-	-	9.70E-5	-	5.50E-5	9.40E-5
X_i/X_H	-	-	3.09E-3	-	2.18E-3	3.74E-3
V977 Sco	-	-	-	-	-	5.30E-5
X_i/X_H	-	-	-	-	-	2.10E-3
V443 Sct	-	-	2.40E-5	-	1.80E-5	1.00E-5
X_i/X_H	-	-	7.64E-4	-	7.13E-4	3.98E-4
			Morisset & Pequignot (1996)			
GQ Mus	7.40E-5	7.40E-5	4.50E-5	2.00E-6	1.10E-5	1.30E-5
X_i/X_H	1.78E-3	2.06E-3	1.43E-3	7.03E-5	4.35E-4	5.21E-4
			Arkhipova et al. (2000)			
V705 Cas	-	-	-	-	2.00E-5	6.31E-7
X_i/X_H	-	-	-	-	7.90E-4	2.51E-5